OBSERVATION OF chi_b(2P) TO chi_b(1P) pi+ pi-

A Thesis

Presented to the Faculty of the Graduate School

of Cornell University

in Partial Fulfillment of the Requirements for the Degree of

Master of Science

by

Kenneth Michael Weaver

August 2005

ABSTRACT

We have searched for the di-pion transition $\chi_b' \to \chi_b\ \pi^+\pi^-$ in the CLEO-III sample of Υ(3S) decays in the exclusive decay chain, $\Upsilon(3S) \to \gamma\chi_b'$, $\chi_b' \to \chi_b\ \pi^+\pi^-$, $\chi_b \to \Upsilon(1S)\gamma$, and, finally, $\Upsilon(1S) \to \ell^+\ell^-$. We refute the null hypothesis, finding a signal greater than 6σ deviation from expected background, and thus claim observation of this di-pion decay. For comparisons we have used the well-established channels $\Upsilon(3S) \to \Upsilon(2S)\ \pi^+\pi^-$, with either $\Upsilon(2S) \to \ell^+\ell^-$ or $\Upsilon(2S) \to \gamma\chi_b$. Under reasonable assumptions, we find the two-pion partial width to be, $\Gamma_{\pi^+\pi^-} = (0.80\ \pm 0.21\ \pm\ ^{0.23}_{0.17})$ keV.

BIOGRAPHICAL SKETCH

Before coming to Cornell University in August of 2003, the author graduated from the Science and Humanities Scholars Program at Carnegie Mellon University with a B.S. in physics. He has worked at MIT doing granular flow studies in their Applied Mathematics department. The most expansive summer of his life was spent as a Summer Student at CERN in Geneva, Switzerland. He is leaving Cornell's physics PhD program early, having accepted a position as graduate fellow at the University of Maryland, College Park, in their Creative Writing MFA program.

ACKNOWLEDGEMENTS

Thank you to my parents, friends, and family for supporting me and for being sturdy enough to let me produce my own unique set of opinions and screw-ups. To my advisor, Rich Galik, for being patient with a departing physicist and for getting a better work ethic out of said physicist than anyone preceding him. To our paper committee - Dave Besson, Helmut Vogel, Pete Zweber - for their directions and scrutiny. To Anneliese Schmidt, for all things. To vegetables, libations, and cigars, for their continued support. To Cornell University for their financial assistance and for the time and space to change one's mind. To the CLEO Collaboration for their exquisite data and for their immeasurable support - Brian Heltsley, David Kreinick, Todd Pedlar, Jon Rosner, Tomasz Skwarnicki, and Werner Sun.

TABLE OF CONTENTS

LIST OF TABLES

LIST OF FIGURES

CHAPTER 1

INTRODUCTION & MOTIVATION

1.1 Previous Publications

Initial considerations of this analysis were performed by Tatia Engelmore in 2003-2004, including a presentation at the April APS Meeting in 2004. I've since given recurring presentations at CLEO Collaboration Meetings in September 2004, November 2004, January 2005, and June 2005, as well as a plenary talk to the Collaboration in February 2005. I've also presented preliminary results of this work at the 2005 April APS Meeting, in addition to presenting a practice talk to the Collaboration beforehand.

Rich Galik and I completed an internal CBX note[1] in May 2005, and much of this thesis is constructed around and sampled from the procedure and results contained therein. Galik is currently writing this research up for submission to Physical Review Letters or Phys. Rev. D.

1.2 Decay Channel and Analysis Goals

Because of the large mass of the bottom quark, $\sim 4-5$ GeV, the bottomonium system ($Q\bar{Q} = b\bar{b}$) exhibits a large number of quark-antiquark bound states sitting between the ground state and the Okubo-Zweig-Iizuka threshold[2]. As a result, the available hadronic transitions within this system are accordingly numerous.

Our research here focuses on one particular transition within this system, $\chi_b' \rightarrow \chi_b\ \pi^+\pi^-$, a theoretically-rare decay that has not yet been observed experimentally. Because of the large amount of Υ(3S) data available to the CLEO collaboration (Υ(3S) being the starting point of our decay channel), we are in the

somewhat unique position of being able to attempt to observe this decay, as well as extract additional information about its properties. We in fact do two separate analyses - a *di-pion* analysis and a *single pion* analysis - in an attempt to isolate our signal process from background events. The bottomonium system, with our di-pion transition and main background process separately indicated, is shown in Figure 1.1 below.

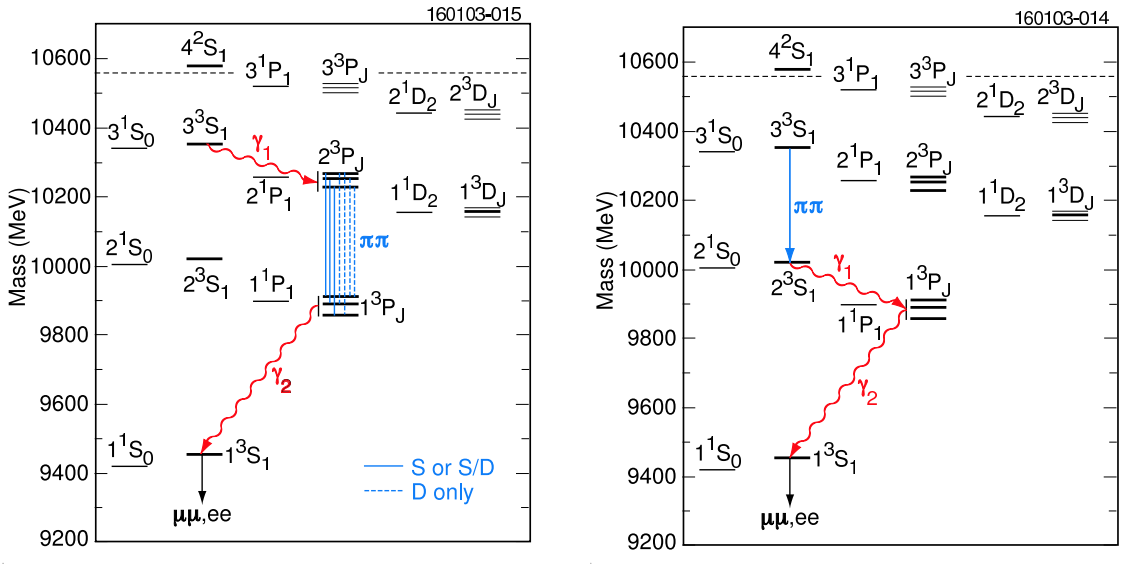

Figure 1.1: The bottomonium system ($Q\bar{Q} = b\bar{b}$), with our exclusive decay channel (left) and main background process (right) highlighted.

Particle physicists extensively use spectroscopic notation to represent different excitations within these quark-antiquark meson systems. Each state can be indicated in the form $n^{2S+1}L_J$, where n is the radial quantum number (the number of nodes exhibited by the radial wave function, plus one), S is the total spin of the system (0 or 1), L is the relative orbital angular momentum (L=0 is indicated by "S", L=1 by "P", L=2 by "D", and so forth), and J is the system's total angular momentum ($\mathbf{J}=\mathbf{L}+\mathbf{S}$) [3]. The spectroscopic notation for χ_b' is 2^3P_J, and for χ_b is 1^3P_J. Since J can assume values of L-1, L, or L+1 (0, 1, or 2, in our case), both

of these states are in fact triplet states, and there exist nine conceivable di-pion transitions between the two states. In a later section, we explain our reasoning for limiting our inquiry here to only two of these transitions.

There are approximately 5.81 million Υ(3S) decays in the CLEO data and, using current branching fractions from the Particle Data Group[4], we can calculate the number of expected transitions through these χ_b' states. These values are shown in Table 1.1.

Table 1.1: The PDG E1 branching fractions from the Υ(3S) to the χ_b' triplet, and the expected number of such decays in the CLEO-III resonance running.

J	B(Υ(3S)$\rightarrow \gamma\chi_b'$)	# of χ_b' ($\times 10^3$)
0	$5.4 \pm 0.6\%$	314
1	$11.3 \pm 0.6\%$	657
2	$11.4 \pm 0.8\%$	662

Beginning with particle decay data taken from the CLEO-III detector, we use a processing program (written in an amalgam of C++ and Fortran programming languages; much of it inherited) to make certain requirements of possible signal events. We will be looking at an *exclusive* decay process, beginning from the Υ(3S) state and decaying through our signal transition. Our exclusive decay channel begins with an E1 transition from this state, Υ(3S)$\rightarrow \gamma\chi_b'$; χ_b' then decays by our signal process, $\chi_b' \rightarrow \chi_b\ \pi^+\pi^-$; χ_b gives off a photon in another E1 transition, to Υ(1S); Υ(1S) then decays to two leptons, either electrons (e^+e^-) or muons ($\mu^+\mu^-$). Our *exclusive* decay channel (indicated also in Fig. 1.1) can be summarized as follows:

$$\Upsilon(3S)\rightarrow \gamma_1\chi_b' \rightarrow \gamma_1\pi^+\pi^-\chi_b \rightarrow \gamma_1\pi^+\pi^-\gamma_2\ \Upsilon(1S)\rightarrow \gamma_1\pi^+\pi^-\gamma_2\ell^+\ell^-.$$

Very little is known about these χ_b' and χ_b triplet states, and the only observed transitions from them are photonic emissions to the Υ(1S) and Υ(2S) states[4], as well as an ω transition to Υ(1S)[5]. The di-pion emission characterizing our signal process is in fact the dominant hadronic transition for these heavy quarkonia states. While such transitions have already been observed among the singlet $^3S_1$ states, it has not yet been studied for the triplet $\eta_c^{'} \to \pi\pi\eta_c$ transition, nor the $\chi_b' \to \chi_b\, \pi^+\pi^-$ process under investigation here. These hadronic decays are characterized by the emission of two soft (low-energy) gluons, which then hadronize to form the observed pions. This two-step process is illustrated in Figure 1.2.

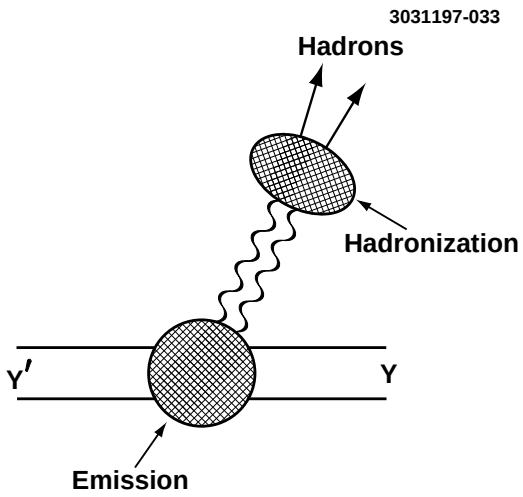

Figure 1.2: The di-pion transition between χ_b' and χ_b is characterized by a two-step process in which two soft gluons are emitted and hadronize into the observed pions.

Because the $\chi_b' \to \chi_b\ \pi^+\pi^-$ decay process has never before been observed experimentally and its branching fractions between the triplet states are not known, we established the following three goals for our analysis, in descending likelihood of success:

- (1) Refute the null hypothesis - namely, that predicted background rates

from other decay processes could account for whatever was seen from data.

- (2) Calculate a partial width for this process from the number of observed signal events.

- (3) Present the di-pion mass spectrum ($m_{\pi\pi}$) of those events judged to be coming from our decay process.

Refuting the null hypothesis was of primary importance. An estimate to the number of expected background events seen in data is determined by analyzing likely background processes, as well as looking at generic decays starting from the Υ(3S) state. Once we look at data, this number (and its corresponding error) is compared to the number of events actually seen. A deviation of greater than 3σ corresponds, in particle physics, to "evidence" of this process, while a deviation of greater than 5σ from background (with appropriate cross-checks, etc.) allows one to claim "observation" of the analyzed decay process. There are a number of ways to improve the observed signal, including adding restrictions to certain event criteria that, while slightly reducing the efficiency with which we observe signal events, cuts more dramatically into background processes than signal, leaving a clearer picture of any observed signal events.

Since we end up looking at multiple transitions between the χ_b' and χ_b triplet states, a measurement of the partial width ends up being the easiest quantity to extract that indicates the frequency with which this process occurs. Dividing the partial width of a particular decay by the full width of the initial state (both typically given in units of energy) gives the branching fraction for a particular decay process. In this analysis, we use calculated full widths of the initial χ_b' states to extract a partial width value.

Lastly, and of most theoretical concern, is the issue of the di-pion mass spectrum for this process. The di-pion mass is obtained by summing the 4-vectors of the two charged pions (either directly or indirectly, as will be shown), then taking the invariant mass of this quantity. In this analysis we will present the di-pion mass distribution for those events likely to have come from our signal process.

1.3 Discussion of $m_{\pi\pi}$ Theory

The discovery of the heavy-quark systems - the J/ψ particle[6][7], its corresponding excitations, and, later, the bottomonium system - was the first opportunity for scientists to test the theoretical predictions of *perturbative* quantum chromodynamics (QCD)[3]. Earlier experimental study, involving positronium and the bound states of lighter quarks, served as a testing ground for quantum *electrodynamics* and quantum field theory, and, in a very similar way, study of the heavy-quark systems allows us to better understand quantum *chromodynamics* and the strong interaction[3].

Because of the low energies available to these emitted pions, study of the di-pion mass distributions for transitions within these bottomonium and charmonium systems allows physicists to better understand further theoretical considerations: *nonperturbative* QCD[3], as well as considerations of QCD confinement structure and the gluonic content of lighter hadrons[8]. These is a strong level of interest towards examining these soft-gluonic transitions within the theory community, since this is essentially an additional step in evaluating and refining the theory describing these quarkonia systems. Our concern within this introduction will focus on the nonperturbative theories available and the di-pion mass spectra seen in other heavy-quarkonia hadronic transitions, such as $\psi' \rightarrow \pi^+\pi^- J/\psi$ and transitions

between the bottomonium singlet states.

Early studies into the $\psi' \rightarrow \pi^+\pi^- J/\psi$ decay[9] showed a di-pion mass spectrum that did not correspond to the expectation from phase space[10] (as had been seen previously for $\eta' \rightarrow \pi\pi\eta$ decays[11], for instance). The di-pion mass spectrum - plotted between (at the lower end) twice the pion mass and (at the higher end) the available energy between the two transition states - showed a prominent high-mass peak. Similar results were seen for the neutral pion transitions, as well as in the Υ(2S)$\rightarrow \pi\pi\Upsilon$(1S) modes[8] and Υ(3S)$\rightarrow \pi\pi\Upsilon$(2S) modes[12] (see [4] and [13] for additional references). The left graph in Figure 1.3 shows di-pion mass spectra for Υ(3S)$\rightarrow \pi\pi\Upsilon$(2S) from earlier CLEO-II[12, 14] and CLEO-III[15] analyses.

The development of theories to understand this high-mass peak in hadronic transitions is well-documented by both the BES Collaboration paper on $\psi' \rightarrow \pi^+\pi^- J/\psi$[10], as well as the CLEO Collaboration paper on Υ(2S)$\rightarrow \pi\pi\Upsilon$(1S)[8], and these summaries will be followed closely here. Initial calculations to determine the decay amplitude for the $\psi' \rightarrow \pi^+\pi^- J/\psi$ process (thus giving a theoretical distribution for the di-pion spectrum) were carried out by Brown and Cahn[16] and Voloshin[17], both of which assumed chiral symmetry breaking to be a negligible effect and used partially conserved axial vector currents (PCAC) to generate theoretical distributions with a high-mass peak. (PCAC involves a slight non-conservation of axial vector currents due to interaction between a particle's physical mass and the surrounding gluonic fields; it was initially developed to handle weak interactions, but is equally applicable here.) Brown and Cahn demonstrated that unbroken chiral symmetry reduced the problem to essentially three basic momentum-dependent parameters. Using early data on the $\psi' \rightarrow \pi\pi J/\psi$ decay[9], which suggested that the decay was isotropic, they concluded that two

of these parameters (both producing angular correlations) were necessarily small, and set them equal to zero for ease of calculation. This gave an isotropic decay amplitude that peaked for large values of $m_{\pi\pi}$. Cahn later revisited this question of removing the anisotropic parameters [18] - which are not inherently prohibited by unbroken chiral symmetry - and calculated angular distributions for the ψ' decay based upon partial-wave amplitudes diagonal in orbital and spin angular momentum. Yan later demonstrated that one of these two anisotropic parameters was indeed nonzero[2].

All of the analyses mentioned in the previous paragraph were specifically concerned with the $\psi' \rightarrow \pi\pi J/\psi$ mass spectrum. Discovery of the many hadronic transitions within the $b\bar{b}$ spectrum caused many later theoretical arguments to assume more generality. As mentioned previously, the hadronization producing the two pions seen in our signal process occurs in a two-step process: (1) the emission of two gluons, and (2) the production of charged pions due to the interaction between the gluon color field and the vacuum[8]. As these two processes can be handled somewhat independently of one another, theory explaining this hadronization process was also factorized. Gottfried[19] was able to provide the theoretical underpinnings for much of the first part - the emission of two gluons - by making an analogy between transitions seen in nuclear processes (changing electric fields) to transitions between the heavy quarkonium states (changing color fields). In spite of the two gluons being 'soft', and thus nonperturbative, Gottfried demonstrated that the multipole expansions used to handle non-relativistic electromagnetic fields could also be used to handle the gluonic fields in the strong interactions of these heavy $Q\bar{Q}$ systems. Because these states are so massive, the leading-order terms converge rapidly, and he was able to provide a number of testable predictions

governing these hadronic decays. Concerning a handling of the second part of the hadronization, he pleaded ignorance. Yan[2] and (later) Zhou and Kuang[20] would use these same expansion techniques (as well as the quark-confining string model[21]) to make predictions regarding transition rates and a parametrization of the $m_{\pi\pi}$ spectrum in the Υ system. In referencing the high-mass peak seen in most of these transitions, we will most frequently reference the Yan distribution, which includes two nonzero terms in its parametrization.

The second step of this process, the calculation of the pion hadronization matrix element, was calculated by Voloshin and Zakharov[22] and, in a revised analysis[10], by Novikov and Shifman [23]. An alternative approach was used here - also invoking current algebra, PCAC, and gauge invariance, as before[8] - but starting from 'first principles' of quantum chromodynamics instead of using phenomenological results from the $\psi' \rightarrow \pi\pi J/\psi$ decay. Voloshin and Zakharov calculated transition ratios by using triangle anomalies in the axial-current divergence and in the trace of the energy-momentum tensor. Their results agreed with findings for both the $\psi' \rightarrow \pi\pi J/\psi$ decay and the known high-mass-peaked Υ decays. The Voloshin-Zakharov, Novikov-Shifman, and Yan (with higher-order terms included) models all produce very similar fits to the observed $m_{\pi\pi}$ spectra[10].

A deviation from this simple high-mass peak distribution is observed in the $\Upsilon(3S) \rightarrow \pi\pi\Upsilon(1S)$ transitions[12, 24], which shows a double peak in $m_{\pi\pi}$. Results from CLEO-III for the charged[25] and neutral[15] modes of this decay are shown in the right graph of Figure 1.3.

Like the high-mass peak behavior previously, a great deal of theoretical effort went into trying to understand this double-bump feature in the $\Upsilon(3S) \rightarrow \pi\pi\Upsilon(1S)$ decays. Unlike the $\psi' \rightarrow \pi\pi J/\psi$, $\Upsilon(3S) \rightarrow \pi\pi\Upsilon(2S)$, and $\Upsilon(2S) \rightarrow \pi\pi\Upsilon(1S)$

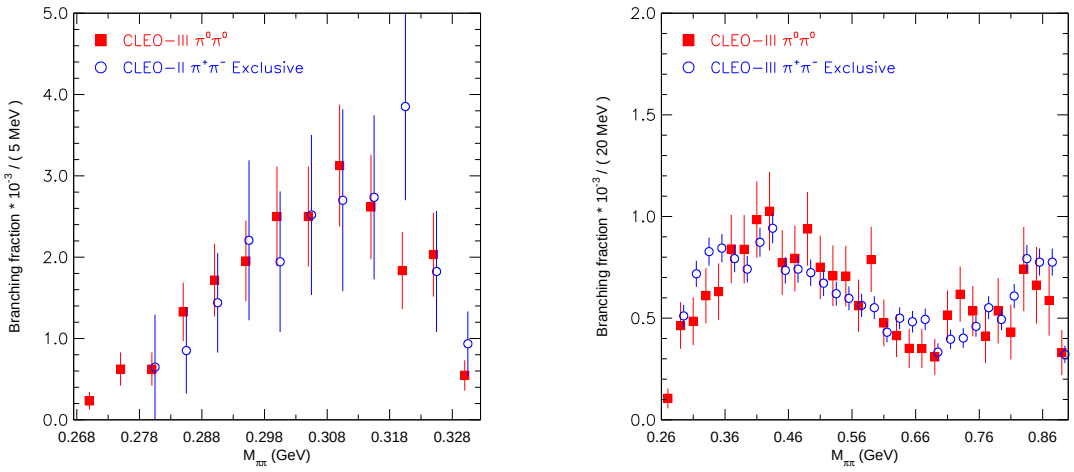

Figure 1.3: On the left are the $m_{\pi\pi}$ spectra for the $\Upsilon(3S) \rightarrow \pi\pi\Upsilon(2S)$ decays, from earlier CLEO analyses. The right figure shows the double-peaked feature of the $\Upsilon(3S) \rightarrow \pi\pi\Upsilon(1S)$ spectrum, again from CLEO-III data.

transitions (all of which have 300-600 MeV available between the transitional states), ∼900 MeV is available to the two pions in this decay. A number of unsuccessful attempts were made to theoretically explain this double-peak feature, including the introduction of $\pi\pi$[26] and $\Upsilon\pi$[27] resonances, corrections to the multipole-expansion techniques, considerations of final-state interactions, and even the suggestion of a narrow four-quark isovector state between the $\Upsilon(3S)$ and $\Upsilon(2S)$ masses[27]. None of these techniques were able to produce the double-bump shape seen in data. Only later did Moxhay[28], by having the $\pi\pi$ and $\Upsilon\pi$ resonances (coupled-channel amplitudes) and the multipole expansion amplitudes interfere, reproduce the behavior seen in the $\Upsilon(3S) \rightarrow \pi\pi\Upsilon(1S)$ channel.

More recent studies in the charmonium system also concern themselves with the details of these di-pion transitions. Within the CLEO Collaboration, J.L. Rosner and M. Voloshin have both studied separate aspects of $\psi(3770)$ decaying to $\pi\pi J/\psi$,

hoping to yield more information about this state by studying rates and angular distributions of the decay. X(3872)[29] is also having its di-pion spectra studied, with the goal of assigning appropriate quantum numbers to this newly-discovered state.

To summarize, analyses of these $m_{\pi\pi}$ spectra have provided a number of interesting and illuminating techniques for evaluating theoretical calculations of these quantum-chromodynamical decays. In this analysis we will later present the di-pion mass spectrum for our signal process (albeit with limited yields) - the newest addition to this collection of heavy-quarkonia hadronic transitions. A further consideration would be to study the neutral transition $\chi_b' \rightarrow \pi^0\pi^0\chi_b$, but this will involve six resultant photons (and the associated combinatorics and π^0 reconstructions), and will be undertaken only after completion of the charged analysis.

CHAPTER 2

DATA & MONTE CARLO

2.1 CLEO-III Datasets

Our analysis follows previous CLEO analyses - Pedlar[5], Engelson[15], Skwarnicki [30], Muramatsu[31] - using the $\Upsilon(3S)$ events collected in datasets `data16`, `data17`, and `data22`, which contain a total of $(5.81 \pm 0.12) \cdot 10^6$ $\Upsilon(3S)$ events. The accumulated luminosity of these three datasets is 1.39 fb^{-1}. We also confine our analysis to only those events satisfying the `radlep` subcollection, the details of which are provided in Appendix A. This is a standard subcollection for low-multiplicity (events with few charged tracks), exclusive analyses.

2.2 Likely Transitions

As mentioned in the introduction, we limit our investigation to focusing on only two of the transitions between the χ_b' and χ_b triplet states. In our CBX note[1], Galik shows that the 0-to-1 and 1-to-0 transitions are disallowed (referencing Yan's PCAC considerations[2]) and considers the relative likelihood of the other transitions. Since none of these decays have ever been observed, it is necessary to theoretically consider which transitions will have the largest branching fraction and thus be most likely to appear in the data.

Both the χ_b' and χ_b states are iso-scalars and have the same parity (PC=++), which requires the di-pion state to also be an iso-scalar. The iso-vector pions will give the system's wave function a symmetric *isospin* factor; pions are spinless, giving the wavefunction also a symmetric *spin* factor; and pions are bosons, requiring the wave function be symmetric overall. Since the di-pion system will also neces-

sarily be spinless, the total angular momentum of the system will be equal to its orbital angular momentum and will thus assume even values. Since the highest available energy between these two triplet states is 409 MeV (2-to-0) - only 129 MeV greater than twice the pion rest mass - the S-wave transitions between χ_b' and χ_b will dominate over D-wave transitions and so forth. Galik[1] calculates the energy penalty for D-wave transitions to be around 400 MeV, much greater than the maximum of 129 MeV available. The BES Collaboration[10] calculates D/(S+D) for $\psi' \rightarrow \pi\pi J/\psi$ to be only about 18%, while Steve Pappas[32] presented preliminary results indicating this ratio to be consistent with zero for the Υ(3S)$\rightarrow \pi\pi\Upsilon$(2S) decay. In all cases, those transitions with S-wave components prove to be significantly more likely than those with only D-wave possibilities. This reduces our considerations to the 0-to-0, 1-to-1, and 2-to-2 transitions.

Also to be considered is the overall branching fraction to the χ_b' state (from Υ(3S)) and from the χ_b state (to the Υ(1S)). (In all cases, the Υ(1S) state decays to two leptons independently of the J and J' values.) The PDG sets an upper limit on the $\chi_{b0} \rightarrow \gamma\Upsilon$(1S) branching fraction of 6%; half of this value is used for our calculations. Regardless of the value used, however, the 0-to-0 decay is expected to be accessed significantly less often than either the 1-to-1 or 2-to-2 decays.

Table 2.1 summarizes the results of these considerations. As noted, 0-to-1 and 1-to-0 are disallowed by symmetry constraints. The remaining $J' \neq J$ transitions occur by D-wave transitions, which are much less prevalent than the S-wave decays. Considering the overall branching fractions to and from the $J' = J$ transitions, we decide to limit our study here to the 1-to-1 and 2-to-2 transitions. We expect these to be, by at least an order of magnitude, our most dominant transitions. This disparity will only be increased as we assign restrictions and cuts specific to

Table 2.1: Summary of the relevant properties of the χ_b' and χ_b triplet states. ΔM represents the mass difference difference between each pair of states. The branching fraction represents the product of $\Upsilon(3S) \rightarrow \gamma\chi_{bJ'}'$ and $\chi_{bJ} \rightarrow \gamma\Upsilon(1S)$.

J'	J	Allowed (Y/N)	ΔM (MeV)	$\mathcal{B}_1 \cdot \mathcal{B}_2$ ($\times 10^{-4}$)	S and/or D Decays	Relative Magnitude of $d\Gamma\ /dm_{\pi\pi}$
2	2	Y	356	251	S or D	$(1' \rightarrow 1) + 0.10 \cdot (0' \rightarrow 2)$
1	1	Y	363	395	S or D	$(0' \rightarrow 0) + 0.25 \cdot (0' \rightarrow 2)$
0	0	Y	372	16	S	"standard"
0	2	Y	320	119	D	largest D-wv
1	2	Y	343	249	D	$0.75 \cdot (0' \rightarrow 2)$
2	1	Y	376	399	D	$0.45 \cdot (0' \rightarrow 2)$
2	0	Y	409	34	D	$0.20 \cdot (0' \rightarrow 2)$
0	1	N	339	189	D	forbidden
1	0	N	395	34	D	forbidden

these two channels.

2.3 Generated Monte Carlo Sets

Monte Carlo allows us to generate simulated sets of particle decays, as well as mimic how these decays travel through the CLEO detector and how they are observed. Generated properly, they allow us to examine a decay channel before we look at real events from data. In spite of the $\chi_b' \rightarrow \chi_b\ \pi^+\pi^-$ process never having been previously observed, by knowing the masses and appropriate quantum numbers governing this transition, we can analyze this process and assign appropriate restrictions and cuts to distinguish between our process and likely background processes. We do all of these things before ever looking at events from actual data.

We use Monte Carlo samples for both our 1-to-1 and 2-to-2 signal transitions, as well as for decay processes likely to appear as background in this analysis. Because the final state of our exclusive decay channel includes two photons, two

low-momentum charged tracks (from the pions), and two high-momentum charged tracks (from the $\Upsilon(1S) \rightarrow \ell^+\ell^-$ transition), we choose background decay channels likely to produce a similar final collection of observed particles. We also run our processor over collections of generic $\Upsilon(3S)$ and continuum $\Upsilon(3S)$ and $\Upsilon(4S)$ events. Scaling each of these contributions accordingly will allow us to predict the amount of background and signal events we expect to observe in our signal regions when looking at actual data events.

The details of each of these Monte Carlo samples are itemized below, with the final Υ state of each specific Monte Carlo sample symmetrically decaying to two leptons (50% e^+e^-, 50% $\mu^+\mu^-$). The π^0's decay to two photons ~99% of the time. The details of each sample are also summarized below in Table 2.2.

- Signal Monte Carlo, $\Upsilon(3S) \rightarrow \gamma_1\chi_b' \rightarrow \gamma_1\pi^+\pi^-\chi_b \rightarrow \gamma_1\pi^+\pi^-\gamma_2\Upsilon(1S)$

  Initial considerations of our signal process used Monte Carlo samples generated earlier by Tatia Engelmore, using `data16` calibrations and Model 31. This method of Monte Carlo generation suffered numerous setbacks, resulting in oddly-sized compilations of 1-to-1 (3347 events) and 2-to-2 transitions (3626 events). We used these Monte Carlo samples to get initial boundaries for our signal region in the di-pion analysis and compare efficiency values between these samples and newer samples of Monte Carlo to assess systematic errors in our generation techniques.

  Newer Monte Carlo samples were generated with `data22` calibrations and Model 1, with the help of Pete Zweber. 10,000 events of both 1-to-1 and 2-to-2 transitions were produced, starting from a virtual photon with $E(\gamma^*) = m(\Upsilon(3S))$ and $\sigma(E(\gamma^*)) \sim 12$ keV, consistent with the energy and full width of the $\Upsilon(3S)$ state. The energy spread of the initial state is very important,

as this determines the width of the energy distribution for the initial E1 transition, $\Upsilon(3S) \rightarrow \gamma_1 \chi_b'$. Galik calculated that the introduction of crossing angles and high/low annihilations would produce neglible changes to our output variables; as such, the initial momentum of the virtual photon was set to zero.

Altogether, a great deal of effort was put into generating Monte Carlo samples that would best represent how signal events would appear in data. We assess systematic errors and consider recent updates to the χ_b' rest masses[33] (alternately, the energies of the initial E1 transitions) in a later section.

- $\Upsilon(3S) \rightarrow \pi^+\pi^-\Upsilon(2S) \rightarrow \pi^+\pi^-\gamma_1\chi_b \rightarrow \pi^+\pi^-\gamma_1\gamma_2\Upsilon(1S)$

  As shown previously in Figure 1.1, this decay channel serves as the primary background to our signal process, possessing the same decay channel from χ_b onward and having a similar di-pion recoil mass and E1 transition energy. Tomasz Skwarnicki provided us with 40,000 Monte Carlo events for this decay channel, and this process will often be referred to as the "Tomasz" process. PDG[4] values are used for the input branching fractions, with the $\chi_{b1} \rightarrow \gamma\Upsilon(1S)$ rate set at 3% (half the PDG upper-limit of 6%, with a 90% confidence level). We additionally use this decay channel as a check to our efficiency and fitting procedure in the *single pion* analysis and as a check of background levels in both our *di-pion* and *single pion* analyses. In all cases, this decay channel proved to be the more difficult to isolate from our signal process.

- $\Upsilon(3S) \rightarrow \pi^+\pi^-\Upsilon(2S)$

  While this Monte Carlo sample contributes a negligible amount of back-

ground to our signal regions, it proves useful in demonstrating the capabilities of our processor in the *di-pion* analysis. This low-background, high-yield study shows that we are in fact able to detect soft di-pion transitions accurately and produce compatible efficiencies between data and Monte Carlo. This check, using the 60,000 events available within the Monte Carlo sample, is handled in a later section. This decay channel will often be referred to as the "existence" channel.

- $\Upsilon(3S) \rightarrow \gamma_1 \chi_b' \rightarrow \gamma_1 \omega \Upsilon(1S) \rightarrow \gamma_1 \pi^+ \pi^- \pi^0 \Upsilon(1S)$

  Todd Pedlar[5] provided us with an enormous sample of 375,000 Monte Carlo events for this process, recently found to have a surprisingly large branching fraction. Since it is a newly discovered decay, it will not be contained within the generic $\Upsilon(3S)$ Monte Carlo. The J=0 transition is kinematically forbidden, so Pedlar's Monte Carlo contains only J = 1,2 transitions, using appropriate PDG values. For all events, ω strictly decays to $\pi^+\pi^-\pi^0$. This process - which has the same initial E1 transition as our signal channel, but rarely a second photon of sufficiently high energy to pass our required γ_2 cut of 300 MeV - is referred to as the "omega" channel.

- $\Upsilon(3S) \rightarrow \pi^+ \pi^- \Upsilon(2S) \rightarrow \pi^+ \pi^- \pi^0 \pi^0 \Upsilon(1S)$

  The neutral di-pion transition here provides the necessary photons, although too many; we require two or three photons in both the *di-pion* and *single pion* analyses. We call this decay channel the "missing γ" channel. Our Monte Carlo sample contains 5,000 of these events, which will only occasionally manage to mimic the two photons present in our signal process.

- Generic $\Upsilon(3S)$ Monte Carlo

Table 2.2: Monte Carlo samples used for this analysis, including signal (1-to-1 and 2-to-2), likely specific backgrounds, and generic and continuum Υ(3S) samples.

Type	Name	$N(\times 10^3)$	Notes
$\Upsilon(3S) \to \gamma_1 \ \pi^+\pi^- \ \gamma_2\Upsilon(1S)$	Signal	27	only $J = J' = 1, 2$
Standard CLEO Υ(3S)	Generic	4450	1x data16/17
$\Upsilon(3S) \to \pi^+\pi^-\Upsilon(2S)$	Existence	60	Existence proof
$\Upsilon(3S) \to \pi^+\pi^- \ \gamma_1 \ \gamma_2\Upsilon(1S)$	Tomasz	40	E1 rates as in PDG
$\Upsilon(3S) \to \gamma_1 \ \omega\Upsilon(1S)$	Omega	375	100% $\omega \to \pi^+\pi^-\pi^0$
$\Upsilon(3S) \to \pi^+\pi^- \ \pi^0\pi^0\Upsilon(1S)$	Missing γ	5	
Continuum *udsc*	Continuum	15908	4x data16/17

Generic Υ(3S) Monte Carlo samples were available only for `data16` and `data17`. These generic collections take into account all previously-known transitions beginning from the Υ(3S) state. The available samples represent "1x" data, at an accumulated luminosity of 711 pb^{-1}. We flag those events beginning with the $\Upsilon(3S) \to \pi^+\pi^-\Upsilon(2S)$ transition, as these are already accounted for by the specific Monte Carlo samples listed above.

- Continuum Υ(3S) and Υ(4S) Monte Carlo

  The continuum Υ(3S) Monte Carlo samples were also available only for `data16` and `data17`, but represent "4x" data. Instead of being $b\bar{b}$ output, these samples represent four-flavor *udsc* continuum events, with energy near the Υ(3S). Since one can't necessarily control what flavor quarks originate from the e^+e^- annihilations within the accelerator, these Monte Carlo samples account for "junk" events likely to be seen in data. While their contributions to the signal regions are likely to be quite small, care needs to be taken that such backgrounds are properly accounted for. Bhabha and radiative Bhabha events, it should be noted, are not included within these

Monte Carlo samples.

We additionally run our processor over the available Υ(4S) continuum Monte Carlo (of which there is a much greater supply) and scale down its background contribution by the ratio of luminosities (Υ(4S) to Υ(3S)), producing a more accurate estimate of the continuum's background contribution within the Υ(3S) data.

CHAPTER 3

TWO SEPARATE ANALYSES

Because our signal processes are expected to have exceptionally small branching fractions (on the order of 1% for each $\chi_b' \to \chi_b \, \pi^+\pi^-$ transition), it proved necessary to use two separate and distinct analyses to filter out a signal. In both cases we look at the *exclusive* analysis described earlier, with a final state consisting of two photons, two low-momentum charged tracks (pions), and two high-momentum charged tracks (leptons). The main distinction between our two analyses hinges upon whether both or only one of the soft pion tracks are actually reconstructed by the CLEO detector.

Our initial analysis, the "di-pion" analysis, looked only at events where both pion tracks were found. Even with soft (highly-efficient) cuts to maximize efficiency, our processor returned only about 12% of Monte Carlo events with *both* pion tracks reconstructed. This low efficiency arises as a consequence of the silicon vertex detector within CLEO-III; soft pions are often absorbed or scattered at large angles, making reconstruction difficult. Because the energy available to the two pions is, at most, ∼200 MeV above their combined rest mass, frequently one or both of these charged pions is missed by the detector.

Our second analysis takes this pion-detection difficulty into account and instead looks at events where only one of the two soft pions was found. This analysis is referred to as the "single pion" analysis. In this case, our initial efficiency (the percentage of Monte Carlo events passing our processor and exhibiting one low-momentum charged track) increases to ∼26%, more than doubling the initial efficiency of the di-pion analysis. Here the general philosophy is to reconstruct the missed pion by using the observed photons and charged tracks and subtracting

their contributions away from the beam four-momentum to see what remains.

Both of these analyses are explained in further detail below.

3.1 Di-Pion Analysis

As both our signal process and the main background process (Fig. 1.1) have the same decay channel proceeding from the χ_b state downward, cuts on γ_2 and the final lepton pair will not be useful for isolating our signal from this "Tomasz" background. In both the *di-pion* and *single pion* analyses, the initial E1 photon transition and the di-pion transition itself will have to provide the variables we cut on most sharply to distinguish between these two event sources. In both analyses, we formulate two-dimensional measurement regions to encapsulate the areas where our signal events are most likely to appear, one side of which will be E_1, the energy of the lower-energy photon γ_1. For the *di-pion* analysis, the second dimension of this signal region will be provided by the recoil mass against the two-pion system, as given by the following equation:

$$M_{rec} \equiv \sqrt{(\mathcal{P}_{3S} - \mathcal{P}_{\gamma 1})^2} - \sqrt{(\mathcal{P}_{3S} - \mathcal{P}_{\gamma 1} - \mathcal{P}_{\pi+} - \mathcal{P}_{\pi-})^2} \; . \tag{3.1}$$

where $\mathcal{P}_{3S}$ is the beam energy 4-vector. This variable - essentially $M(\chi_b') - M(\chi_b)$, for our di-pion transition - has the best resolution compared to similar variables and offered the most promise for being able to distinguish between our signal process and the Tomasz background process. (Also, we don't wish to use the di-pion invariant mass as a cut, as showing the unperturbed distribution of $m_{\pi\pi}$ is one of the main goals of this analysis.) Our two-dimensional measurement regions (we in fact create three distinct regions, to keep track of backgrounds and so forth) for the *di-pion* analysis are formed by plotting the variables E_1 versus M_{rec}. Specific

boundaries for these regions and additional applied cuts will be discussed in a later section.

3.2 Single Pion Analysis

In the *single pion* analysis, only one of the pion tracks is reconstructed by the CLEO-III detector. Here our final state consists of two photons, a single low-momentum pion track, and the two high-momentum lepton tracks. The general philosophy behind this analysis is to reconstruct the missing pion ourselves using the available four-vectors from the observed particles and the beam energy, as well as available fitting techniques and internal CLEO software.

Looking at the distributions of E_1 and E_2 (the energies of the low- and high-energy photons in our exclusive decay channel), we determine the average energy sum for these two photons, weighted between the 1-to-1 and 2-to-2 values by their respective branching fractions (i.e., the 1-to-1 value is weighted more heavily, by approximately a factor of two). Using this fixed energy sum (518.3 MeV), we then take events with two or three photons and find the best overall pairing: extracting a fit value (χ^2), scaling the photons' 4-vectors to the appropriate energy, and outputting their unfit energies to our "ntuple" (the n-dimensional collection of data variables output for each event passing our processor requirements). We use the lower unfit photon energy, E_1^{unfit}, again as one of the variables in our two-dimensional measurement regions. Further, using the standard CLEO fitting package VXFit, we fit and scale the 4-vectors of the two leptons to the Υ(1S) rest mass, extracting an additional χ^2 fit value.

Having fit the best two photons to a fixed energy and the two leptons to the Υ(1S) mass, and using the 4-vector of the single observed pion, we can subtract

these 4-vectors away from the 4-vector of the beam energy to extract the mass of the missing pion:

$$M_{miss} \equiv \sqrt{(\mathcal{P}_{3S} - \mathcal{P}_{\gamma 1}^{fit} - \mathcal{P}_{\gamma 2}^{fit} - \mathcal{P}_{\Upsilon} - \mathcal{P}_{\pi})^2} \ . \tag{3.2}$$

This missing mass, M_{miss}, will be the second variable in our two-dimensional measurement regions for the single pion analysis - plotting E_1^{unfit} versus M_{miss}. We also have available to us the two extracted fit values: $\chi^2_{\gamma\gamma}$ for the fixed photon energy sum, and χ^2_{Υ} for fitting the two leptons to the Υ(1S) mass. These variables will prove useful for removing background events from our signal region.

More specific information regarding processor criteria, assessed cuts, and how these two-dimensional measurement regions were determined will be elaborated upon in the following sections. We will also discuss the final efficiencies for these two analyses (for both 1-to-1 and 2-to-2 signal processes), before addressing the levels of background we expect upon "opening the box" and looking at actual data.

CHAPTER 4

EVENT REQUIREMENTS, POST-PROCESSOR CUTS, AND MEASUREMENT REGIONS

Within our submitted CBX note[1], Galik provides a theoretical estimate of the $\chi_b' \to \chi_b\ \pi^+\pi^-$ branching fractions for $J' = J = 1, 2$. He estimates a partial width for our process by scaling the partial width of the $\Upsilon(3S) \to \pi^+\pi^-\Upsilon(2S)$ decay by the ratio of the mass differences between each pair of transitional states; this assumes an S-wave dominant process, which seems a reasonable assumption given arguments cited in Chapter 2. The full widths for our signal decays are extracted from the two E1 transitions from each χ_b' state to $\Upsilon(2S)$ and $\Upsilon(1S)$. Because the full width characterizes the initial state itself, this value will be shared between the mentioned E1 transitions and our signal process (separated for $J' = 1, 2$). A branching fraction is then calculated by taking the partial width (which describes a single decay process) and dividing by the full width (which characterizes the initial state; in our case, χ_b').

The product branching fractions (i.e., the entire branching fraction starting from $\Upsilon(3S)$, all the way down to the lepton pair) for our 1-to-1 and 2-to-2 signal transitions are calculated as follows:

$$\mathcal{B}(\Upsilon(3S) \to \gamma_1\pi^+\pi^-\gamma_2\ell^+\ell^-) = (2.2 \pm 0.8) \cdot 10^{-5} \quad [J' = J = 1] \tag{4.1}$$

$$\mathcal{B}(\Upsilon(3S) \to \gamma_1\pi^+\pi^-\gamma_2\ell^+\ell^-) = (1.0 \pm 0.5) \cdot 10^{-5} \quad [J' = J = 2]. \tag{4.2}$$

Galik provides an additional derivation of these values and respective branching fractions, using only published values (instead of the occasional internal CLEO result), in Appendix B of our CBX note. Given these theoretical product branching fractions and starting with $(5.81 \pm 0.12) \cdot 10^6$ $\Upsilon(3S)$ events, we can expect

approximately 128 1-to-1 events and 58 2-to-2 events in all of the CLEO-III $\Upsilon(3S)$ data.

As this is not an exceptionally large quantity of likely signal events, we try to keep our processor and post-processor requirements as loose as possible while maximizing S^2/B. This quantity represents the overall prominence of a signal, and can be better considered as the square of the following quantity: the number of expected signal events divided by the square root (essentially the error) of the number of expected background events. Maximizing this quantity will yield the most effective cuts for discriminating our signal events from background.

We further discuss the cuts made within the processor itself, as well as post-processor cuts and formulated measurement regions, in the following sections.

4.1 Processor Cuts

As mentioned previously, our processor is an amalgam of C++ and Fortran code inherited from Tomasz Skwarnicki, a member of the CLEO Collaboration, currently at Syracuse University. The processor, taken as a whole, is rather general and allows for any number of different analyses to be conducted within the same processor - essentially, if certain particular event criteria are satisfied, then those ntuple entries are filled with the appropriate variables; if not, the ntuple entries remain zeroed or set to their default value. There are, however, certain criteria which must be generally adhered to by any event for it to pass the processor and to have its event data stored in the ntuple (these requirements can of course be changed, but they've remained constant throughout our analyses).

Our processor requires that each event have 2-6 suitable charged tracks (more on this shortly), that two of these tracks have momentum greater than 3.75 GeV/c

and a paired invariant mass within 300 MeV of the $\Upsilon(1S)$ final state (as occurs in our exclusive decay channel), that the remaining charged tracks each have momentum less than 750 MeV/c (corresponding to our soft pion tracks), that there be no more than eight good photons (as defined shortly), and that there be at least two good photons *or* two good soft charged tracks in each event. Skwarnicki also makes a few general requirements regarding missing energy and balanced momentum.

Specific processor restrictions made to the charged tracks in each event are as follows:

- The distance of closest approach to the origin (this is different from the interaction point) must be less than 3 cm. This variable, 'dacd', is shown plotted for lepton and pion tracks in 1-to-1 signal Monte Carlo in Figure 4.1. The figures show 3 cm to be a soft cut on this variable.

- The distance from the interaction point in the longitudinal direction (i.e, the beam axis) must be less than 18 cm. This variable, 'z0', is shown plotted for lepton and pion tracks in Figure 4.2. Again, this cut results in a minimal loss of efficiency. A cut is also made to the error on this quantity, requiring it be less than 25 cm.

- The reduced χ^2 of the fit to the charged track must be less than 100. This represents how reasonably the collection of hits in CLEO's silicon vertex detector and drift chamber match up with the fitted helical path.

- The hit fraction - the number of hits versus the number of hits expected from the fitted helix - must be between 0.5 and 1.2. This number may be larger than one as a result of layered wires registering multiple hits at effectively the same location.

- The momentum of each track must be greater than 50 MeV/c and less than 1.5 times the beam energy (5.17 GeV/c for Υ(3S) events).

- The dip angle of the fitted helix must have $|cos\ \theta| < 0.95$. This establishes a requirement of how tangential a charged track may originate from the beam axis and is coded as $cot\theta < 3.0424$, with the error on this quantity being restricted to 0.5 or less.

- Each track must also be `TRKMAN`-approved. `TRKMAN` is a CLEO track-analysis program which eliminates curlers, *kink*'s (particles which decay in flight, causing a kink and potentially resulting in the same particle's track being counted twice), and makes general, loose track-quality cuts. Initial stages of the analysis by Tatia Engelmore demonstrated that, since the two emitted pions are typically of low momentum, events would often have multiple tracks - *curlers* - that were in fact the same charged pion looping around within the detector. `TRKMAN` helps to eliminate these spurious tracks.

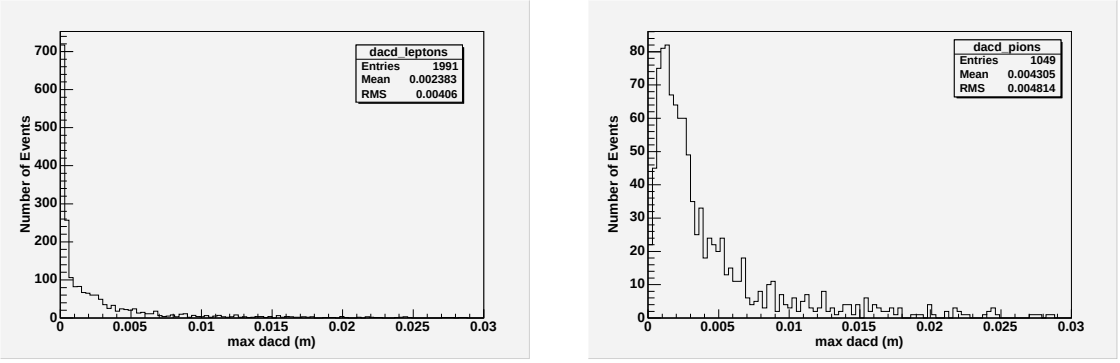

Figure 4.1: Missing distance in the $r-\phi$ plane - 'dacd'. The left plot shows the largest dacd value of the two leptons; the right plot shows the largest value for the two pions. (1-to-1 signal Monte Carlo)

In addition to the charged track requirements listed above (which take care of the two pions and two leptons in our exclusive decay channel), our processor also

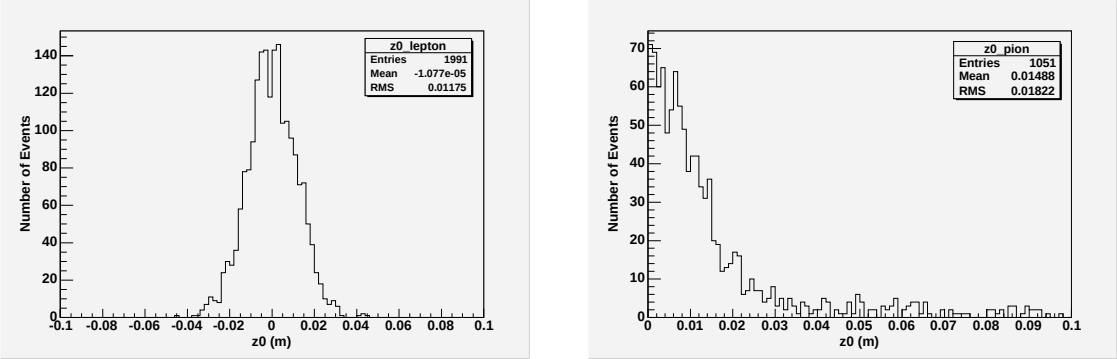

Figure 4.2: Missing distance along z - 'z0'. The left plot shows the z0 distribution for one of the leptons; the right plot shows this same variable plotted for one of the pions. (1-to-1 signal Monte Carlo)

makes certain requirements of the showers (photons passing into the cesium iodide crystal calorimeters of the CLEO detector) within each event. Specific processor cuts to photon showers are as follows:

- Showers resulting from known hot and noisy crystals[34] within the detector are ignored.
- Photons in the inner endcap $|cos\ \theta| > 0.93$ are required to have energies greater than 180 MeV. All other photons are required have energy greater than 60 MeV.
- Charged tracks can lose and deposit energy as they travel through the cesium iodide detector. We do not use showers matching up with charged tracks, based on the CCShowerAttribute `noTrackMatchConReg`.
- Tomasz Skwarnicki provides an algorithm that suppresses fragmented showers resulting from the lepton showers in e^+e^- events.

Additionally, we look only at those events contained within the `radlep` subcollection (further detailed in Appendix A), near the "on-resonance" $\Upsilon(3S)$ beam

energy ($5.1785 < E_{beam} < 5.181 GeV$), and in which the trigger fires (useful only in Monte Carlo), indicating to the CLEO detector that an event has taken place and data collection should commence. All three of these requirements are applied post-processor and for both analyses; they are standard cuts and result in no sizable change to our efficiency. Post-processor cuts specific to each of our two analyses are discussed in the following sections.

4.2 Post-Processor Cuts in the Di-Pion Analysis

For the di-pion analysis we require, most importantly, that each event have exactly two "good" soft tracks, corresponding to the two low-momentum pions of our signal process. We further require that the combined charge of all charged tracks (both leptons and pions) be zero.

Post-processor cuts made to the "good photons" in each event are as follows:

- In the case of events with **two** good photons, we require that both of these photons satisfy an E9/E25 constraint (a measure of how well the shower's lateral profile matches that of an actual photon impacting the CsI detector) to 99% certainty; that both photons *not* originate from bremsstrahlung radiation ($e \rightarrow e\gamma$); and that the highest energy photon have energy greater than 300 MeV. This final requirement was found to eliminate a large amount of background from our signal regions.

- We gain a slight increase in efficiency ($\sim$10%) by also allowing events with **three** "good" photons. With regard to our signal process, these events exhibit one noise photon. Here we require the middle-energy photon have energy greater than 120 MeV, thus putting it outside the observed energy

range for our γ_1 and establishing it as the likely spurious photon. The highest-energy photon is then taken to be γ_2, again requiring it have energy greater than 300 MeV. Otherwise, the same cuts are applied to these photons as to those in the two-photon events.

In addition to the parts of our analysis that specifically try to detect our signal process, we have made a number of checks by running our processor over known decay modes. In one of these analyses, we determined that it would be necessary to make a number of soft (highly-efficient) cuts on variables describing the lepton and pion tracks, to remove QED background in the events with $\Upsilon(1S) \rightarrow e^+e^-$. The selection of soft cuts made for the di-pion analysis are shown below:

- The difference in momentum, Δp, between the two lepton tracks had to be less than 700 MeV/c.
- The softer pion had to have momentum less than 160 MeV/c.
- The harder pion was required to have momentum less than 350 MeV/c.

As indicated in Chapter 3, our best handles on our signal process are E_1 (the energy of the first transition photon) and M_{rec} (the recoil mass against the two-pion system). These variables offer the best resolution for focusing in on our signal process events and distinguishing them from our main backgrounds. Using these two variables, we establish three two-dimensional measurement regions.

One of these - the "Signal" region - forms the area where we are most likely to observe events from our signal process. We perform an S^2/B study in both E_1 and M_{rec} to determine the best boundaries for this region, such that the prominence of any detected signal will be maximized in relation to the expected background.

The boundaries for the "Signal" region in the *di-pion* analysis were determined to be $75 < E_1 < 110$ MeV and $350 < M_{rec} < 375$ MeV.

The second region - the "Tomasz" region - is intended to capture the bulk of the Tomasz events that pass our processor. Since this is a well-understood background channel with known branching fraction, by verifying we can in fact predict the proper number of data events that will fall into this region, we are able to provide a check to our experimental procedure. The boundaries of the "Tomasz" region are shifted slightly higher in E_1 than our signal region and slightly lower in M_{rec}. These two regions do not overlap.

The final region - the "Sideband" region - takes into account all of the events falling into the area *surrounding* these other two regions. It allows us to keep track of any potential nearby backgrounds that might be polluting our "Signal" region. We set lower limits for this region at $E_1 = 60$ MeV (the lowest photon energy allowed by our processor) and $M_{rec} = 280$ MeV (twice the pion rest mass). By estimating the amount of background that falls into this region (from specific and generic Monte Carlo samples), we are able to determine whether any unaccounted background events might require us to alter our background expectation in the other two regions. This will be discussed in more detail in Chapter 7, once we have actually looked at data events.

The boundaries of each of these three regions - in E_1 and M_{rec} - are shown in Table 4.1 below. We also outline the "Signal" and "Tomasz" Region (surrounded by the larger "Sideband" region) in Figure 4.3, with the 1-to-1 and 2-to-2 signal Monte Carlo events plotted in the left figure and the Tomasz background process plotted on the right. We will present expected background levels for each of these regions in the next chapter.

Table 4.1: Boundaries for the three two-dimensional measurement regions in the *di-pion* analysis, plotting E_1 versus M_{rec}, both given in MeV. Note that these regions are entirely separate from one another - events falling into the "Signal" and "Tomasz" regions are not counted in the "Sideband" region.

Region Name	E_1^{min}	E_1^{max}	M_{rec}^{min}	M_{rec}^{max}
Signal	75	110	350	375
Tomasz	90	150	325	340
Sideband	60	200	280	500

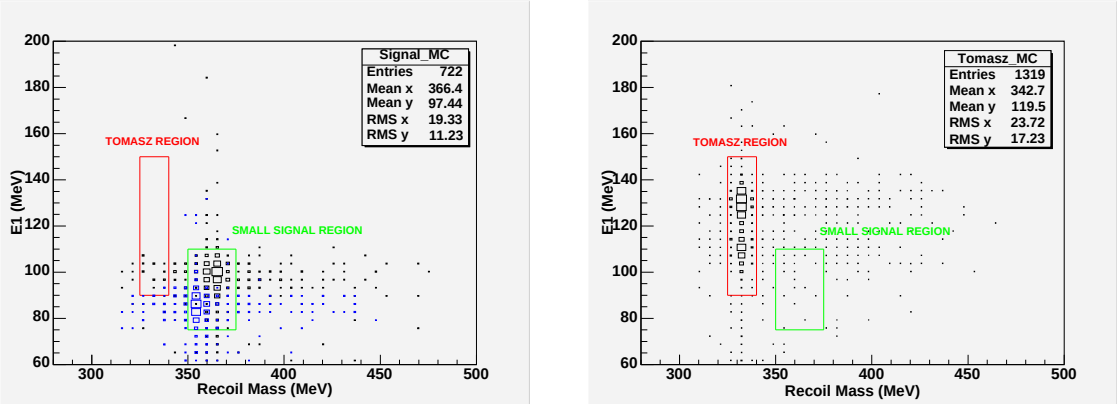

Figure 4.3: Two-dimensional plots of the three measurement regions in the *di-pion* analysis. The left figure shows Monte Carlo events for our 1-to-1 and 2-to-2 signal process. The right figure shows Monte Carlo events for the "Tomasz" background process.

4.3 Post-Processor Cuts in the Single Pion Analysis

Because there is such a significant increase in efficiency - going from events with two soft pion tracks to events in which only one of these soft pions is found - we will discuss the cuts made in our single pion analysis in slightly more detail. This half of the research is certainly the one of highest yield, with efficiencies more than doubled from the di-pion analysis.

Here the CLEO tracking detector is only able to reconstruct one of the low-momentum pion tracks. To get information about the other pion, we begin by

extracting the beam energy for each event, then subtract away all of the other available 4-vectors in our process: the two lepton tracks (which we fit to the $\Upsilon(1S)$ mass using VXFit), the two transitional photons (which we fit to a fixed energy sum), and the lone measured pion. This subtraction will yield, approximately, the 4-vector of the missing pion.

We look only at those events with two or three good photons, again requiring they satisfy E9/E25 to 99% certainty, and determining which two we will use by minimizing a χ^2 fit to an appropriate fixed energy sum. Because the photon energy sum used must be the same for all events analyzed - and because it will not be easy to distinguish between 1-to-1 and 2-to-2 signal events in data - we choose this fixed value by looking at the Monte Carlo distributions for both 1-to-1 and 2-to-2 signal events (with only two photons) and weight the means of these two distributions by the likely relative magnitude of their overall branching fractions. Because the 1-to-1 decay will be our dominant transition, the chosen value of 518.3 MeV is closer to this distribution's mean. The photon energy sums for these two Monte Carlo samples are shown in Figure 4.4. The photon energy sums for our two most prevalent background channels are shown in Figure 4.5.

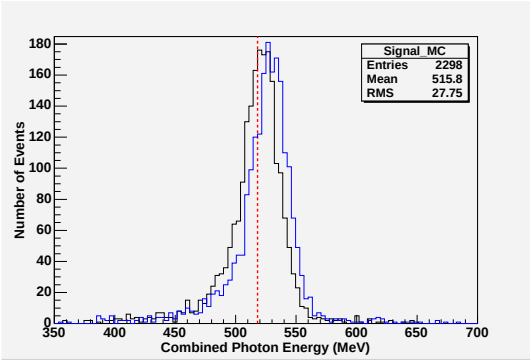

Figure 4.4: The photon energy sum distributions for 1-to-1 and 2-to-2 Monte Carlo. We chose 518.3 MeV, indicated by the dotted line, as the fixed energy sum for our processor's photon fitting procedure.

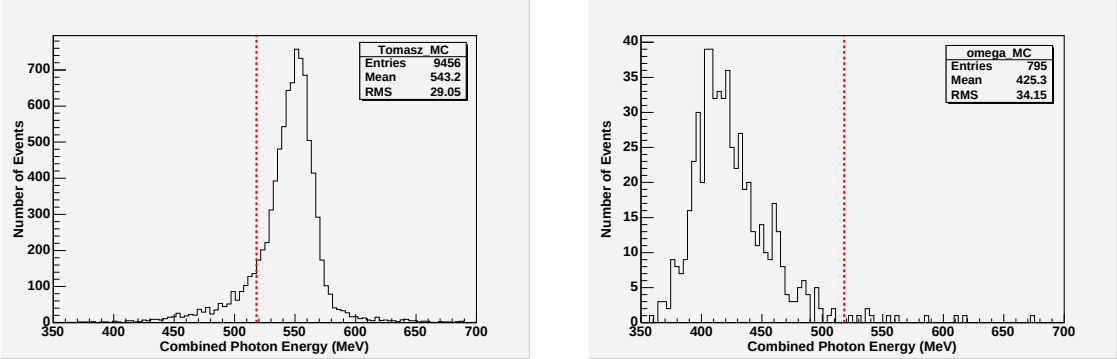

Figure 4.5: The photon energy sum distributions for the "Tomasz" background process (left) and the "omega" background process (right).

We fit the available good photons in each event to this fixed energy sum and choose the pairing that minimizes the χ^2 value for this fit. We scale the 4-vectors of both photons to this fixed total energy, using these new 4-vectors in our evaluation of the missing pion 4-vector.

We also output the unfit energy values of the two photons used: E_1^{unf} and E_2^{unf}. The distributions of these two variables are shown in Figure 4.6. As in the di-pion analysis, we used E_1^{unf} as one of the handle variables in our two-dimensional measurement regions and require that E_2^{unf} be greater than 300 MeV. We also output $\chi^2_{\gamma\gamma}$, the chi-square fit to the energy sum, and will use this variable to eliminate background in our analysis.

The fitting procedure of the two leptons to the Υ(1S) mass is handle by VXFit, a standard fitting package within the CLEO software. Inputting the magnetic field, the two lepton tracks, and the Υ(1S) mass, VXFit fits the decay vertex - outputting an Υ(1S) 4-vector of proper mass and appropriate to the two constituting lepton tracks. It also establishes a χ^2_Υ value for this fit, the distribution of which is plotted in Figure 4.7 for both our signal decays and the "Tomasz" background process.

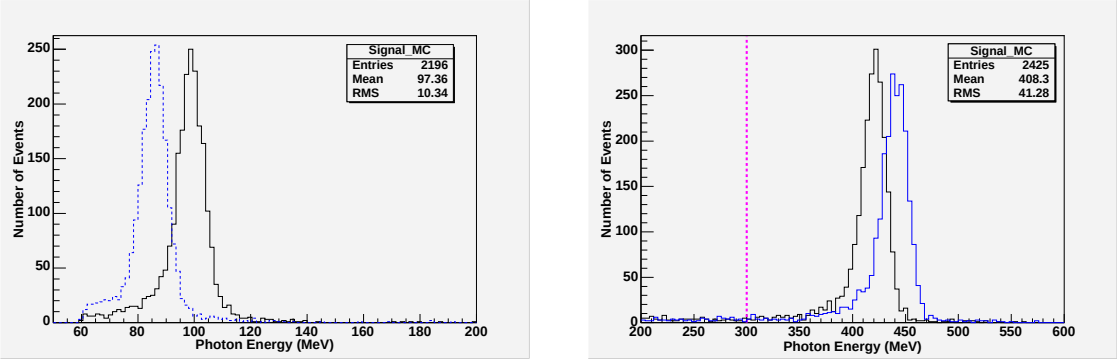

Figure 4.6: E_1^{unf} (left) and E_2^{unf} (right) distributions from the fixed energy sum fitting procedure in the single pion analysis, for 1-to-1 and 2-to-2 Monte Carlo samples. We require E_2^{unf} be greater than 300 MeV (dotted line) and again use E_1^{unf} as a handle variable in our two-dimensional measurement regions.

Because all of the likely background channels to our signal process have this same $\Upsilon(1S) \rightarrow \ell\ell$ final transition, it is not useful for us to cut too tightly on this variable. Performing an S^2/B analysis indicated that a proper cut on this variable requires $\chi^2_\Upsilon < 10$.

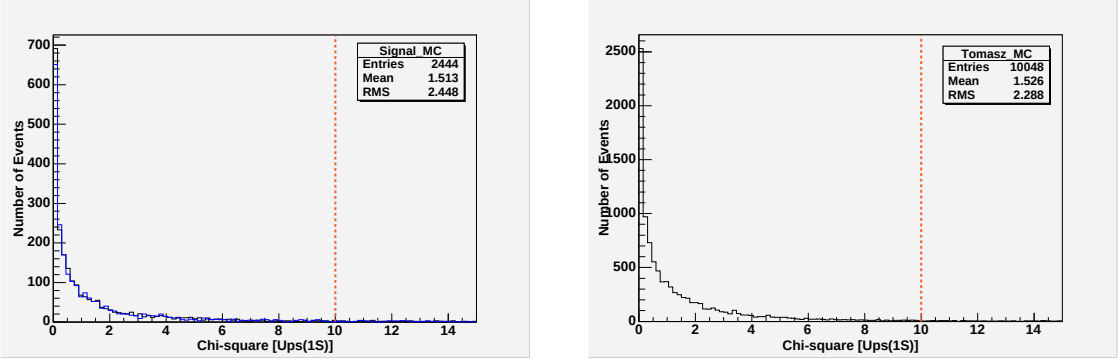

Figure 4.7: Monte Carlo distributions of χ^2_Υ for both our signal transitions (left) and the "Tomasz" background channel (right). Because both decay processes have $\Upsilon(1S) \rightarrow \ell\ell$, we establish a loose cut at $\chi^2_\Upsilon < 10$.

With fitted values for the two transition photons and the $\Upsilon(1S)$ state, the mass of the missing pion can be calculated from Equation 3.2. Distributions of

this variable are shown for 1-to-1 and 2-to-2 signal Monte Carlo in Figure 4.8. Also shown, in Figure 4.9, are the distributions from the "Tomasz" and "Missing γ" Monte Carlo samples.

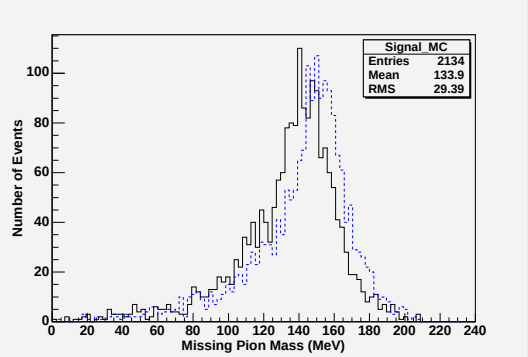

Figure 4.8: Distributions of the missing pion mass in the single pion analysis, for 1-to-1 and 2-to-2 signal Monte Carlo. This variable is the second handle used in the two-dimensional measurement regions for this analysis.

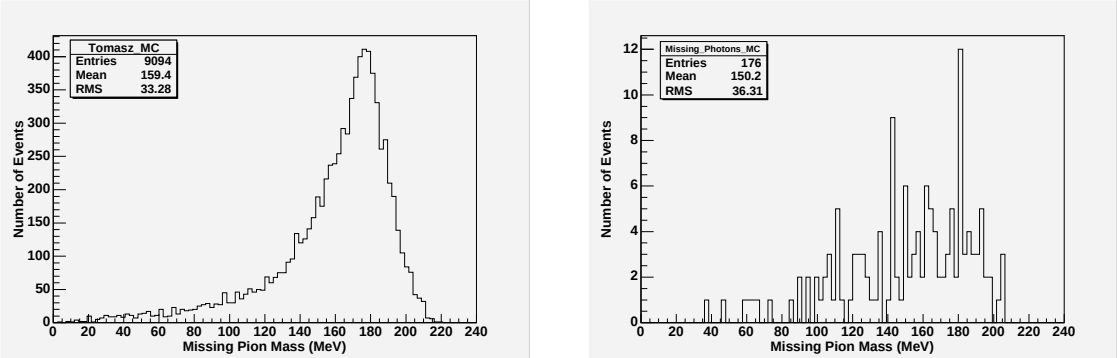

Figure 4.9: Distributions of the missing pion mass for the "Tomasz" (left) and "Missing γ" (right) background processes.

There are then three variables to which we perform an S^2/B study: E_1^{unf}, M_{miss}, and $\chi^2_{\gamma\gamma}$. Note that we already chose a soft cut for $\chi^2_\Upsilon < 10$, as this variable was not helpful in distinguishing our signal process from the main sources of background. The optimal upper and lower bounds of E_1^{unf} and M_{miss} will

determine the area of our "Signal" region for the single pion analysis, and then the best $\chi^2_{\gamma\gamma}$ value will be determined for those events falling within this region.

The results of the S^2/B analysis for E_1^{unf} are shown in Figure 4.10. We first establish the appropriate upper limit for this variable - 105 MeV - without requiring any lower limit, and then determine the appropriate lower boundary, keeping this upper limit fixed. These analyses are shown in the left and right plots, respectively. We find optimal boundaries for our "Signal" region of $75 < E_1^{unf} < 105$ MeV.

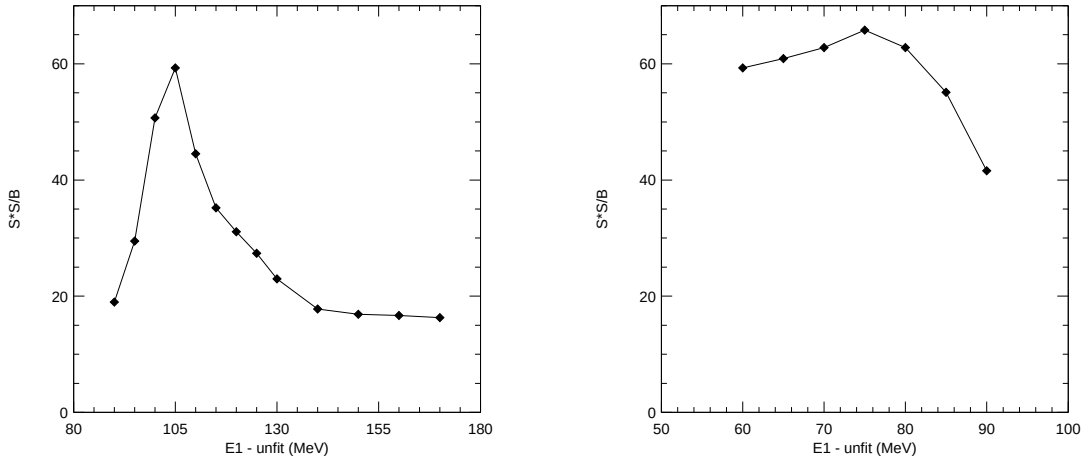

Figure 4.10: S^2/B analysis for E_1^{unf} in the single pion analysis. We establish boundaries at 75 and 105 MeV, where S^2/B is maximized.

This same process is done to M_{miss}: first varying the upper limit of this variable, then finding the appropriate lower limit, keeping the upper boundary fixed. We establish optimal boundaries for this variable of $65 < M_{miss} < 160$ MeV. The results of the S^2/B study are shown in Figure 4.11.

We also looked for any possible correlation between these two variables, E_1^{unf} and M_{miss}, and performed an S^2/B analysis that involved moving the boundary values of our signal region in two dimensions concurrently - to establish that we

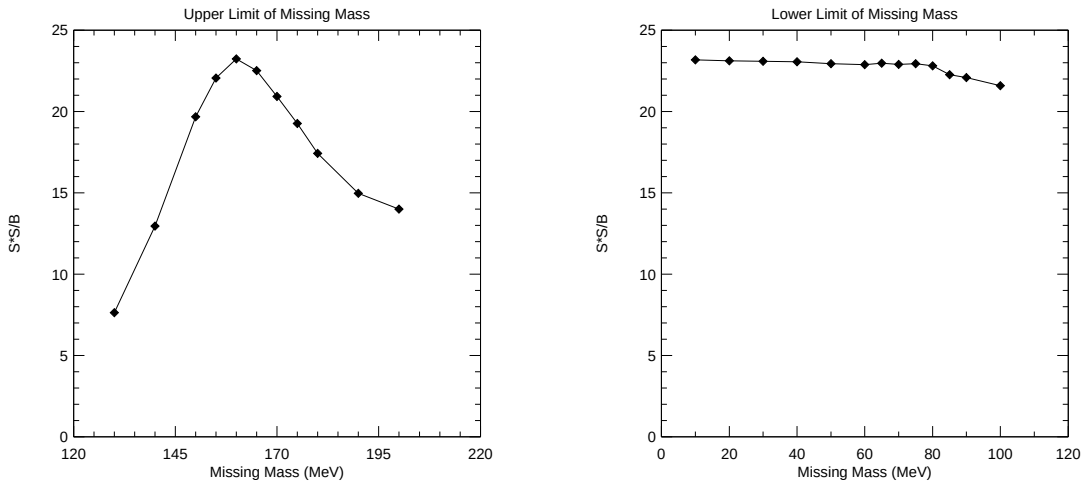

Figure 4.11: S^2/B analysis for M_{miss} in the single pion analysis. We establish boundaries for this variable at 65 and 160 MeV.

did, in fact, have the optimal values overall. This analysis indicated no reason to change the boundary values quoted above.

This leaves the S^2/B analysis for $\chi^2_{\gamma\gamma}$. The S^2/B plot for this variable is generally plateaued between values of 4 and 10, as shown in Figure 4.12. We chose to make the tightest cut within this flat region, at $\chi^2_{\gamma\gamma} < 4$, in an attempt to limit any possible unaccounted background when we actually looked at data.

With all of the cuts and "Signal" region boundaries in place, we again determine appropriate limits for the "Tomasz" and "Sideband" regions, this time for the single pion analysis. The two-dimensional limits for all three of these measurement regions are summarized in Table 4.2. Figure 4.13 outlines these three regions, displaying the distributions of 1-to-1 and 2-to-2 signal Monte Carlo events (left), as well as the "Tomasz" Monte Carlo events (right).

Lastly, as with the di-pion analysis, we assign highly-efficient cuts to the lepton and pion tracks in each event, hoping to limit QED background events slipping

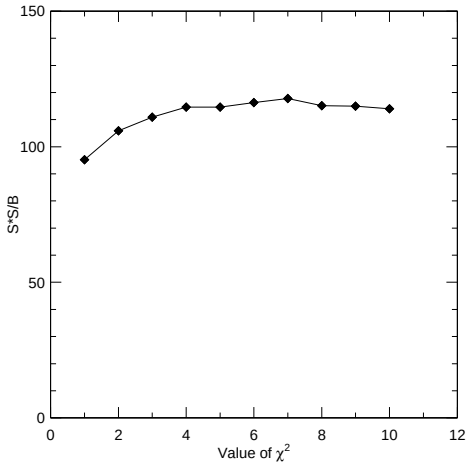

Figure 4.12: S^2/B analysis for $\chi^2_{\gamma\gamma}$ in the single pion analysis. We establish an upper limit for this variable at $\chi^2_{\gamma\gamma} < 4$.

Table 4.2: Boundaries for the three two-dimensional measurement regions in the *single pion* analysis, plotting E_1^{unf} versus M_{miss}, both given in MeV.

Region	E_1^{min}	E_1^{max}	M_{miss}^{min}	M_{miss}^{max}	Comment
Signal	75	105	65	160	
Tomasz	75	140	65	210	Excludes 'Signal' region
Sideband	60	200	0	220	Excludes 'Tomasz' and 'Signal'

into our measurement regions when we actually look at data. The soft cuts for the *single pion* analysis are as follows:

- The difference in momentum, Δp, between the two lepton tracks had to be less than 800 MeV/c.
- The lone observed pion had to have momentum less than 200 MeV/c.
- The di-lepton mass, $m_{\ell\ell}$, had to be between 9.15 and 9.80 GeV. This was a stricter requirement than the cut within the processor.

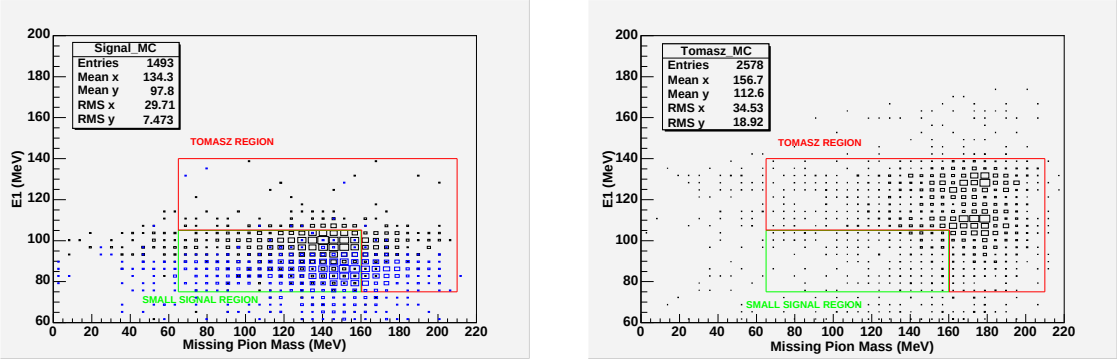

Figure 4.13: Two-dimensional plots of the three measurement regions in the *single pion* analysis. The left figure shows Monte Carlo events for our 1-to-1 and 2-to-2 signal processes. The right figure shows Monte Carlo events for the "Tomasz" background process.

4.4 Efficiency Considerations

"Efficiency" is simply the percentage of events that satisfy any particular requirement made within our analysis. Of primary importance is the overall efficiency - the percentage of 1-to-1 and 2-to-2 signal Monte Carlo events that actually pass through our processor, satisfy the assembled slew of post-processor cuts, and fit within the bounds of our "Signal" regions. Seeing a signal, knowing these values allows us to estimate how many $\chi_b' \rightarrow \chi_b\ \pi^+\pi^-$ events were in the $\Upsilon(3S)$ data originally, and to calculate a partial width (and thus, a branching fraction) for this decay process.

One of our main concerns is how these efficiencies are dependent upon the di-pion mass distribution of the $\chi_b' \rightarrow \chi_b\ \pi^+\pi^-$ decay - a quantity that was discussed to some length in Chapter 1. Monte Carlo naturally throws this di-pion mass distribution according to a simple three-body phase space distribution, though the *real* distribution (that of events to be seen in data) is likely to instead demonstrate the high-mass peak, or perhaps the double-bump behavior, discussed previously.

We checked into the possibility that a skewed di-pion mass distribution could lead to a change in the overall efficiency of our analysis.

We had generated signal Monte Carlo samples appropriate to both `data16` and `data22` calibrations (see Section 2.3). The overall efficiencies for 1-to-1 and 2-to-2 signal Monte Carlo from `data16`, for the di-pion and single pion analyses, are as follows:

$$\epsilon^{\pi\pi}_{1\to1}(\texttt{data16},\Phi_{3bdy}) = (5.0\pm0.4)\%; \quad \epsilon^{\pi\pi}_{2\to2}(\texttt{data16},\Phi_{3bdy}) = (4.2\pm0.3)\% \ ; \ (4.3)$$

and

$$\epsilon^{\pi}_{1\to1}(\texttt{data16},\Phi_{3bdy}) = (12.8\pm0.6)\%; \quad \epsilon^{\pi}_{2\to2}(\texttt{data16},\Phi_{3bdy}) = (10.5\pm0.5)\% \ . \ (4.4)$$

As mentioned earlier, these Monte Carlo samples were generated early on in our investigation, and there had been much difficulty in getting the scripts to run properly.

We more recently generated 10,000 events each for the 1-to-1 and 2-to-2 signal processes, using `data22` calibrations and a more appropriate Υ(3S) energy distribution. These Monte Carlo samples give efficiency values of:

$$\epsilon^{\pi\pi}_{1\to1}(\texttt{data22},\Phi_{3bdy}) = (5.2\pm0.2)\%; \quad \epsilon^{\pi\pi}_{2\to2}(\texttt{data22},\Phi_{3bdy}) = (4.3\pm0.2)\% \ ; \ (4.5)$$

and

$$\epsilon^{\pi}_{1\to1}(\texttt{data22},\Phi_{3bdy}) = (10.9\pm0.3)\%; \quad \epsilon^{\pi}_{2\to2}(\texttt{data22},\Phi_{3bdy}) = (9.6\pm0.3)\% \ . \ (4.6)$$

Note that while the overall efficiencies in the di-pion analysis agree perfectly well between the two datasets, there is some difference between the efficiencies in the single pion analysis. In a later section we assign systematic errors to account for these differences between Monte Carlo samples.

Our primary concern here is to evaluate event efficiency as a function of the di-pion mass, $m_{\pi\pi}$, and determine whether the overall efficiency is changed by introducing a different di-pion mass distribution. Table 4.3 shows this breakdown of efficiencies. The first column separates the $m_{\pi\pi}$ distribution into five bins, while the second column (making use of the *known* distribution of $m_{\pi\pi}$ thrown for this Monte Carlo sample) gives the overall efficiency for events in each bin. These efficiencies are then reweighted according to a high-mass-peaked Yan distribution[15], as well as a flat distribution. The results of this reweighting process are shown for 1-to-1 signal Monte Carlo in the *single pion* analysis.

Table 4.3: Efficiency comparison of the Yan model, 3-body phase space, and a flat distribution in the variable $m_{\pi\pi}$. The first part of table is the efficiency in each bin and the relative weighting for the three models. The last row is the weighted efficiency. This is for the 1-to-1 transition in the *single pion* analysis; 2-to-2 and di-pion analyses are similar.

Bin in $m_{\pi\pi}$	$\epsilon(\%)$	Φ_{3bdy}	Yan	flat
0.279-0.296	8.2 ± 0.7	0.13	0.07	0.20
0.296-0.312	12.2 ± 0.7	0.22	0.16	0.20
0.312-0.329	12.2 ± 0.7	0.26	0.24	0.20
0.329-0.346	11.1 ± 0.6	0.24	0.30	0.20
0.346-0.363	9.3 ± 0.7	0.15	0.23	0.20
Weighted Eff	–	10.9%	10.9%	10.6%

From Table 4.3, we calculate new values for the overall efficiency by reweighting the binned efficiencies by the appropriate di-pion mass distributions. The predicted overall efficiencies for the Yan distribution are as follows:

$$\epsilon^{\pi\pi}_{1\to1}(\texttt{data22}, \text{Yan}) = (5.0 \pm 0.2)\%; \quad \epsilon^{\pi\pi}_{2\to2}(\texttt{data22}, \text{Yan}) = (4.3 \pm 0.2)\% \ ; \quad (4.7)$$

and

$$\epsilon^{\pi}_{1\to1}(\texttt{data22}, \text{Yan}) = (10.9 \pm 0.3)\%; \quad \epsilon^{\pi}_{2\to2}(\texttt{data22}, \text{Yan}) = (9.3 \pm 0.3)\% \ . \quad (4.8)$$

These values are shown for comparison. In a later section we assign systematic errors in our overall efficiencies resulting from different di-pion mass distributions.

In Table 4.4 we show how the processor efficiency and the efficiency of each individual post-processor cut contribute to the overall efficiency in the di-pion analysis. The left column of numbers keeps track of the net efficiency - the cumulative effect of all requirements up to that point - while the right column gives the efficiency of each individual cut, as compared to the overall efficiency from the section of cuts before it. (Note that there is some correlation between these cuts, such that the product of the relative efficiencies in the right column is not necessarily equal to the final efficiency.) Similarly, Table 4.5 shows this breakdown for the single pion analysis, which has roughly twice the overall efficiency of the di-pion analysis.

Table 4.4: Table of efficiencies for the *di-pion* analysis, in percent. The left column shows the cumulative efficiency of all cuts applied up to that point, while the right column gives the relative efficiency of each cut within that section. Efficiencies shown are for 1-to-1 signal Monte Carlo. The 2-to-2 channel yields similar results.

Criterion	Cum. Eff.	Own Eff.	Comment
Processor throughput	49	49	
E_{bm} is at Υ(3S)	49	100	By definition, in MC
MC trigger fires	48	98	Not an issue for data
In `radlep` subcl	48	99.9	See appendix
2 "soft" trks, with $Q_{tot} = 0$	11	**22**	Toughest criterion
2 or 3 quality showers; one with $E > 300$ MeV	7.3	79	`NOBREM`, E9/E25; minimize noise
E1: [75,110] MeV	6.7	92	"Signal" region
Recoil Mass: [350,375] MeV	5.2	77	"Signal" region
Soft cuts on leptons/pions	5.2	99.6	Minimize effect of noise
Overall	5.2	—	4.3% for $J = J' = 2$

Lastly, it is known that Monte Carlo underestimates the width of the photon resolution in the barrel of the CLEO detector by about 15% [35]. By expanding

Table 4.5: Table of efficiencies for the *single pion* analysis, in percent. The left column shows the cumulative efficiency of all cuts applied up to that point, while the right column gives the relative efficiency of each cut within that section. Efficiencies shown are for 1-to-1 signal Monte Carlo. The 2-to-2 channel is similar.

Criterion	Cum. Eff.	Own Eff.	Comment
Processor throughput	49	49	
E_{bm} is at Υ(3S)	49	100	By definition, in MC
MC trigger fires	48	98	Not an issue for data
In `radlep` subcl	48	99.9	See appendix
1 "soft" track	25	**53**	Higher % than di-pion
2 or 3 quality showers; one with $E > 300$ MeV	24	49	`NOBREM`, E9/E25; minimize noise
$\chi^2_\Upsilon < 10$	22	93	χ^2 of lepton fit to Υ(1S)
$\chi^2_{\gamma\gamma} < 4$	17	76	χ^2 of photon energy sum
E_1^{unf}: [75,105] MeV	15	89	"Signal" region
M_{miss}: [65,160] MeV	10.9	73	"Signal" region
Soft cuts on leptons/pions	10.9	100	Minimize effect of noise
Overall	10.9	—	9.6% for $J = J' = 2$

our E_1 transition energies by this amount (since nearly all of our photons are barrel photons), we see a slight decrease to both the 1-to-1 and 2-to-2 efficiencies: relative changes of 4.5% and 1.5%, respectively. For later calculations in the single pion analysis (such as a final evaluation of our signal's partial width), we will use the weighted average of the efficiences seen in `data16` and `data22`, scaled down by these relative changes due to photon resolution differences. This gives final efficiency values, for the single pion analysis, as follows:

$$\epsilon^{\pi}_{1\to1}(\texttt{avg.}, \Phi_{3bdy}) = (10.8 \pm 0.3)\%; \quad \epsilon^{\pi}_{2\to2}(\texttt{avg.}, \Phi_{3bdy}) = (9.7 \pm 0.3)\% \ . \qquad (4.9)$$

CHAPTER 5

ANALYSIS OF LIKELY BACKGROUNDS

5.1 Initial Background Rate Calculations

From the available Monte Carlo samples - specific backgrounds, generic Υ(3S), and continuum Υ(3S) - one can use known branching fractions and determined efficiencies to predict the number of background events falling into each of our measurement regions. These calculations will be the focus of this section.

For specific Monte Carlo samples, we first calculate the total number of these events actually expected in the available Υ(3S) data. From here, we multiply this quantity by the overall efficiency for that process, calculated for each separate measurement region, to establish the expected background rate. Errors are propagated throughout.

As an example, we here evaluate the expected level of background contributed by the "Tomasz" process to the three measurement regions in the *di-pion* analysis. The branching fractions for this decay channel, quoted from the Particle Data Group[4], are as follows:

$$\mathcal{B}_{\pi\pi} \equiv \mathcal{B}(\Upsilon(3S) \to \pi^+\pi^-\Upsilon(2S)) = (2.8 \pm 0.6)\%$$

$$\mathcal{B}_{\gamma 1,2} \equiv \mathcal{B}(\Upsilon(2S) \to \gamma_1\chi_{b2}) = (7.0 \pm 0.6)\%$$

$$\mathcal{B}_{\gamma 1,1} \equiv \mathcal{B}(\Upsilon(2S) \to \gamma_1\chi_{b1}) = (6.8 \pm 0.7)\%$$

$$\mathcal{B}_{\gamma 1,0} \equiv \mathcal{B}(\Upsilon(2S) \to \gamma_1\chi_{b0}) = (3.8 \pm 0.6)\%$$

$$\mathcal{B}_{2,\gamma 2} \equiv \mathcal{B}(\chi_{b2} \to \gamma_2\Upsilon(1S)) = (22 \pm 4)\%$$

$$\mathcal{B}_{1,\gamma 2} \equiv \mathcal{B}(\chi_{b1} \to \gamma_2\Upsilon(1S)) = (35 \pm 8)\%$$

$$\mathcal{B}_{1S\ell\ell} \equiv \mathcal{B}(\Upsilon(1\mathrm{S}) \to \ell^+\ell^-) = (4.96 \pm 0.12)\%$$

Note that, by convention, the final branching fraction uses twice the value and error of the $\Upsilon(1\mathrm{S}) \to \mu^+\mu^-$ branching fraction (muon and electron final states should contribute equally here, and the current muon value has a smaller error). Also, the Particle Data Group cites an upper limit of 6% to the $\chi_{b0} \to \gamma_2\Upsilon(1S)$ branching fraction; by CLEO convention, the Skwarnicki Monte Carlo uses a value of $(3\pm1)\%$ for this decay. The overall branching fraction of this process, B(Tomasz), is then calculated to be:

$$\mathcal{B}(Tomasz) = \mathcal{B}_{\pi\pi} \cdot \Sigma[\mathcal{B}_{\gamma 1,j} \cdot \mathcal{B}_{j,\gamma 2}] \cdot \mathcal{B}_{1S\ell\ell} = (5.6 \pm 1.5) \cdot 10^{-5}. \qquad (5.1)$$

Starting with $(5.81 \pm 0.12) \cdot 10^6$ $\Upsilon(3\mathrm{S})$ events, we would expect 325 ± 87 Tomasz events in the available CLEO-III data.

We need to then calculate the overall efficiencies for this decay channel in each of the three measurement regions in the di-pion analysis. Starting with 40,000 Tomasz Monte Carlo events, with all post-processor cuts and region boundaries applied, we see 456 events in the "Sideband" region (corresponding to $(1.1 \pm 0.1)\%$ efficiency), 808 events in the "Tomasz" region ($(2.0 \pm 0.1)\%$ efficiency), and 26 events in the "Signal" region ($(0.1 \pm 0.1)\%$ efficiency). Multiplying each of these values by the expected number of Tomasz events in data, we predict 3.7 ± 1.1 Tomasz events in the "Sideband" region, 6.6 ± 1.9 events in the "Tomasz" region, and 0.2 ± 0.1 events in the "Signal" region.

This manner of calculation is performed for all of the contributing backgrounds, for both the di-pion and single pion analyses, and is also tabulated separately for the $\Upsilon(1\mathrm{S}) \to e^+e^-$ and $\Upsilon(1\mathrm{S}) \to \mu^+\mu^-$ final states (which yield slightly different overall efficiencies); this latter part allows us to keep better track of the levels of

unaccounted QED background, which will be much more pronounced in the e^+e^- final states.

Because we had generic Υ(3S) Monte Carlo samples only from `data16` and `data17`, their background contributions were scaled up to the appropriate number of Υ(3S) events expected in data (i.e., scaled up to include the `data22` contribution as well). Note that the *continuum* Υ(3S) Monte Carlo did not contribute any events to our measurement regions.

Tables 5.1 and 5.2 show the individual contributions from each of these sources in the three measurement regions for the di-pion and single pion analyses, respectively. In the case of background sources which produced events only in the "Sideband" region, we assumed this distribution was generally uniform and extrapolated this small background contribution into the other measurement regions by the ratios of their areas.

5.2 Upsilon(4S) Continuum Data Check

In addition to the available Υ(3S) continuum Monte Carlo, which is "4x" data, there is a wealth of continuum events available from the Υ(4S) *data*. The utility here is that the Υ(4S) data will include both *udsc* continuum events *and* QED events, the latter of which are not included in our Υ(3S) continuum Monte Carlo samples. The only change made to our analysis was to remove the post-processor restriction that the beam energy be at the on-resonance Υ(3S) energy peak. Unlike the methods applied within the next section, here we did *not* perform any rescaling to the event variables; for our purposes, the Υ(3S) and Υ(4S) energies are adequately close to one another (within 230 MeV).

We ran over the Υ(4S) data collections `data5-data14`, which had an accu-

Table 5.1: Summary table of background contributions in the *di-pion* analysis. As noted earlier, the "Sideband" region does not include either of the other two measurement regions. The third column represents the $\Upsilon(1S) \rightarrow \ell^+\ell^-$ final states: muons and electrons combined ($\ell\ell$), muons only ($\mu\mu$), and electrons only (ee).

Channel	Name		Sideband	Tomasz	Signal
$\Upsilon(3S)$	generic	$\ell\ell$	11.1 ± 3.7	0.3 ± 0.1	0.3 ± 0.1
$\Upsilon(3S) \rightarrow \pi^+\pi^-\Upsilon(2S)$	existence	$\ell\ell$	–	–	–
$\Upsilon(3S) \rightarrow \pi^+\pi^-\gamma_1\gamma_2\Upsilon(1S)$	Tomasz	$\ell\ell$	3.7 ± 1.1	6.6 ± 1.9	0.2 ± 0.1
$\Upsilon(3S) \rightarrow \gamma_1\omega\Upsilon(1S)$	omega	$\ell\ell$	1.7 ± 0.3	–	–
$\Upsilon(3S) \rightarrow \pi^+\pi^-\pi^0\pi^0\Upsilon(1S)$	missing γ	$\ell\ell$	2.6 ± 0.9	1.6 ± 0.6	–
Continuum (scaled 4S)	continuum	$\ell\ell$	3.6 ± 1.8	0.1 ± 0.1	0.1 ± 0.1
$\Upsilon(3S)$	generic	$\mu\mu$	6.1 ± 2.7	0.2 ± 0.1	0.2 ± 0.1
$\Upsilon(3S) \rightarrow \pi^+\pi^-\Upsilon(2S)$	existence	$\mu\mu$	–	–	–
$\Upsilon(3S) \rightarrow \pi^+\pi^-\gamma_1\gamma_2\Upsilon(1S)$	Tomasz	$\mu\mu$	2.0 ± 0.6	3.7 ± 1.1	0.1 ± 0.1
$\Upsilon(3S) \rightarrow \gamma_1\omega\Upsilon(1S)$	omega	$\mu\mu$	0.9 ± 0.2	–	–
$\Upsilon(3S) \rightarrow \pi^+\pi^-\pi^0\pi^0\Upsilon(1S)$	missing γ	$\mu\mu$	1.4 ± 0.6	0.9 ± 0.4	–
Continuum (scaled 4S)	continuum	$\mu\mu$	1.8 ± 1.3	0.1 ± 0.1	0.1 ± 0.1
$\Upsilon(3S)$	generic	ee	4.9 ± 2.5	0.2 ± 0.1	0.2 ± 0.1
$\Upsilon(3S) \rightarrow \pi^+\pi^-\Upsilon(2S)$	existence	ee	–	–	–
$\Upsilon(3S) \rightarrow \pi^+\pi^-\gamma_1\gamma_2\Upsilon(1S)$	Tomasz	ee	1.7 ± 0.5	2.9 ± 0.8	0.1 ± 0.1
$\Upsilon(3S) \rightarrow \gamma_1\omega\Upsilon(1S)$	omega	ee	0.8 ± 0.2	–	–
$\Upsilon(3S) \rightarrow \pi^+\pi^-\pi^0\pi^0\Upsilon(1S)$	missing γ	ee	1.2 ± 0.5	0.7 ± 0.4	–
Continuum (scaled 4S)	continuum	ee	1.8 ± 1.3	0.1 ± 0.1	0.1 ± 0.1

mulated luminosity of 8,600 pb^{-1}; this is 4.7 times the luminosity of the $\Upsilon(3S)$ datasets. We do not make any distinction here between on-resonance and off-resonance events.

The $\Upsilon(4S)$ events falling into the measurement regions of our di-pion and single pion analyses are shown in Figure 5.1. In the di-pion analysis (left), we see 18 total events falling into our three regions. Assuming a uniform distribution, we can extract an estimate of the levels of continuum background in $\Upsilon(3S)$ data: first by scaling down by the ratios of each individual region's area to that of the whole region, and then by scaling down again by the factor of 4.7 from the increased

Table 5.2: Summary table of background contributions in the *single pion* analysis. Note that the "Sideband", "Tomasz", and "Signal" regions are entirely separate from one another. The third column represents the $\Upsilon(1S) \rightarrow \ell^+\ell^-$ final states: muons and electrons combined ($\ell\ell$), muons only ($\mu\mu$), and electrons only (ee).

Channel	Name		Sideband	Tomasz	Signal
$\Upsilon(3S)$	generic	$\ell\ell$	0.9 ± 0.9	0.3 ± 0.3	0.1 ± 0.1
$\Upsilon(3S) \rightarrow \pi^+\pi^-\Upsilon(2S)$	existence	$\ell\ell$	–	–	–
$\Upsilon(3S) \rightarrow \pi^+\pi^-\gamma_1\gamma_2\Upsilon(1S)$	Tomasz	$\ell\ell$	2.3 ± 0.7	16.6 ± 4.8	2.1 ± 0.6
$\Upsilon(3S) \rightarrow \gamma_1\omega\Upsilon(1S)$	omega	$\ell\ell$	–	–	–
$\Upsilon(3S) \rightarrow \pi^+\pi^-\pi^0\pi^0\Upsilon(1S)$	missing γ	$\ell\ell$	1.9 ± 0.7	0.3 ± 0.2	–
Continuum (scaled 4S)	continuum	$\ell\ell$	0.2 ± 0.2	–	–
$\Upsilon(3S)$	generic	$\mu\mu$	–	–	–
$\Upsilon(3S) \rightarrow \pi^+\pi^-\Upsilon(2S)$	existence	$\mu\mu$	–	–	–
$\Upsilon(3S) \rightarrow \pi^+\pi^-\gamma_1\gamma_2\Upsilon(1S)$	Tomasz	$\mu\mu$	1.3 ± 0.4	8.9 ± 2.6	1.1 ± 0.3
$\Upsilon(3S) \rightarrow \gamma_1\omega\Upsilon(1S)$	omega	$\mu\mu$	–	–	–
$\Upsilon(3S) \rightarrow \pi^+\pi^-\pi^0\pi^0\Upsilon(1S)$	missing γ	$\mu\mu$	1.2 ± 0.5	0.1 ± 0.1	–
Continuum (scaled 4S)	continuum	$\mu\mu$	–	–	–
$\Upsilon(3S)$	generic	ee	0.9 ± 0.9	0.3 ± 0.3	0.1 ± 0.1
$\Upsilon(3S) \rightarrow \pi^+\pi^-\Upsilon(2S)$	existence	ee	–	–	–
$\Upsilon(3S) \rightarrow \pi^+\pi^-\gamma_1\gamma_2\Upsilon(1S)$	Tomasz	ee	1.0 ± 0.3	7.7 ± 2.2	1.0 ± 0.3
$\Upsilon(3S) \rightarrow \gamma_1\omega\Upsilon(1S)$	omega	ee	–	–	–
$\Upsilon(3S) \rightarrow \pi^+\pi^-\pi^0\pi^0\Upsilon(1S)$	missing γ	ee	0.7 ± 0.4	0.1 ± 0.1	–
Continuum (scaled 4S)	continuum	ee	0.2 ± 0.2	–	–

luminosity. This same procedure is done for the lone $\Upsilon(4S)$ event appearing in the measurement regions of the single-pion analysis (shown on the right).

These new estimates are given in Tables 5.1 and 5.2 as the scaled continuum $\Upsilon(4S)$ contributions. Because the $\Upsilon(3S)$ continuum Monte Carlo samples predicted no continuum events populating our measurement regions, we use the scaled $\Upsilon(4S)$ numbers as an upper estimate.

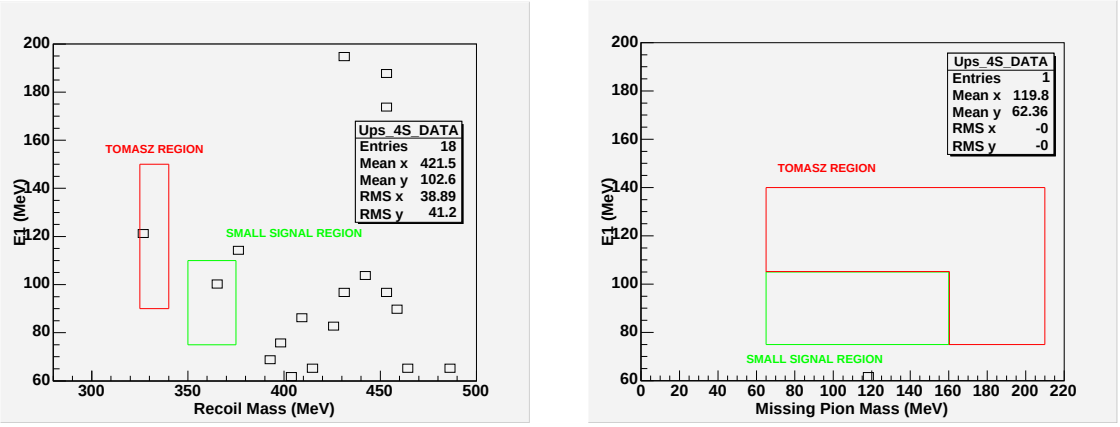

Figure 5.1: Events falling into our di-pion (left) and single pion (right) measurement regions for the Υ(4S) continuum data check.

5.3 Upsilon(2S) Resonance Process Check

There was also some concern that there could exist some unaccounted-for resonance process that would populate our signal region when we actually looked at Υ(3S) data. To address this possibility, one of our paper committee members, David Besson, suggested that we run our processor over the available Υ(2S) data, scaling transitions occuring between the Υ(3S) and Υ(1S) states by the appropriate energy ratio. For the Υ(2S) data, this factor would be $[M(\Upsilon(3S)) - M(\Upsilon(1S)]/[M(\Upsilon(2S)) - M(\Upsilon(1S)] = 1.6$.

One can refer to the available CBX note[1] for further details of this check. The important aspects are as follows: (1) the minimum photon energy requirements and fitted energy sum values within the processor are scaled *down* by 1.6, (2) all outputted variables from the photons and pions in each event are scaled *up* by this factor of 1.6, to correspond to the cuts we already have in place, and (3) the beam energy in the missing pion reconstruction procedure is fixed to the Υ(3S) energy. Taken as a whole, these scalings allow for us to look at transitions between the Υ(2S) and Υ(1S) states as though they were occuring between the Υ(3S) and

Υ(1S) states. Any unknown resonance process that could appear in Υ(3S) data should also manifest itself here.

The results from the Υ(2S) resonance check are shown in Figure 5.2. Only three events appear in our measurement regions, none of which fall into the "Signal" region. One of these - looking at available variables in our ntuple - is likely to come from a π^0 or η transition. Noting that the number of available Υ(2S) and Υ(3S) events are approximately equal, we conclude that if some unaccounted-for resonance process does exist, it will *not* populate our "Signal" region when we run over Υ(3S) data.

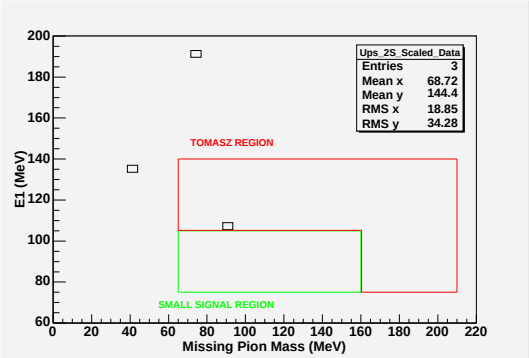

Figure 5.2: Events falling into our single pion measurement regions for the Υ(2S) resonance process check.

This concludes our analysis of background processes likely to appear in the measurement regions of our di-pion and single pion analyses.

CHAPTER 6

DI-PION AND SINGLE PION ANALYSIS CHECKS

6.1 Efficiency Check for the Di-Pion Analysis

As a further check to our di-pion analysis, we modify our processor to run over the $\Upsilon(3S) \rightarrow \pi^+\pi^-\Upsilon(2S) \rightarrow \pi^+\pi^-\ell^+\ell^-$ channel. We typically refer to this decay process as the "existence" channel, in that it allows us to confirm whether our processor can in fact appropriately identify soft di-pion transitions, and thus whether or not we can consider our run over data (looking for our signal process) to be conclusive.

Galik evaluates an overall branching fraction for this process within the CBX note[1], recombining older CLEO results[14, 24] and CUSB values cited in the PDG[4]. Taking the weighted average of these values, with the neutral modes removed (when possible), he calculates an overall branching fraction of:

$$\mathcal{B}(existence) = (1.10 \pm 0.12) \cdot 10^{-3} \ . \tag{6.1}$$

From a starting point of $(5.81 \pm 0.12) \cdot 10^6$ $\Upsilon(3S)$ events, we can thus expect 6380 ± 700 of these "existence" events in data.

We necessarily modify our processor to require an $\Upsilon(2S) \rightarrow \ell^+\ell^-$ final state instead of the $\Upsilon(1S)$ transition in our regular analyses. We also remove the requirement for events to have at least two good photons, since there are no photons in the decay channel of the "existence" process. Our initial post-processor cuts are similar to before - beam energy on-resonance, `radlep` subcollection, trigger fires (in Monte Carlo) - and we further require that we see no more than one photon in each event. Our initial efficiency from Monte Carlo is $\sim 5.5\%$, and our initial look at data (plotting the recoil mass and separating muon and electron final states) is shown in Figure 6.1.

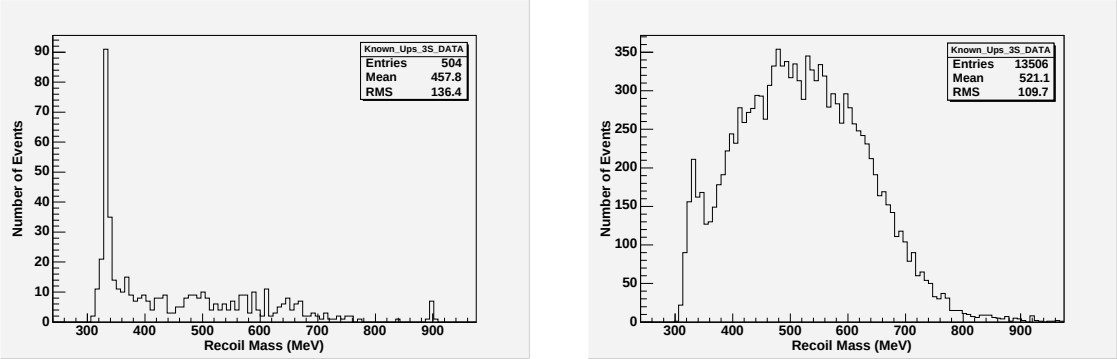

Figure 6.1: Initial look at muon (left) and electron (right) events in the our "existence" check of the di-pion analysis.

We see an enormous amount of QED background in the electron channel. To remove these events, we added a number of additional soft cuts to the lepton and pion track requirements (we do this also in our di-pion and single pion analyses). The cuts are as follows:

- The difference in momentum, Δp, between the two lepton tracks had to be less than 250 MeV/c.
- Our cut on the di-lepton invariant mass, $m_{\ell\ell}$, was tightened to be between 9.9 and 10.2 GeV.
- The softer pion had to have momentum less than 100 MeV/c.
- The harder pion was required to have momentum less than 150 MeV/c.

Taken altogether, these cuts serve to greatly eliminate QED background from our electron "existence" events in data.

Applying these new cuts, we get the Monte Carlo distributions (for muon and electron events) shown in Figure 6.2. These two distributions exhibit a double-Gaussian shape, which we fit using RooFit, a fitting package that runs within

the Root environment. The two Gaussians are distinguished as either "narrow" or "wide," and their fit values from Monte Carlo are given in the left half of Table 6.1. We see an overall combined efficiency for the muon and electron events of $(4.33 \pm 0.08)\%$. [Or (4.22 ± 0.09) %, reweighting for the Yan distribution.]

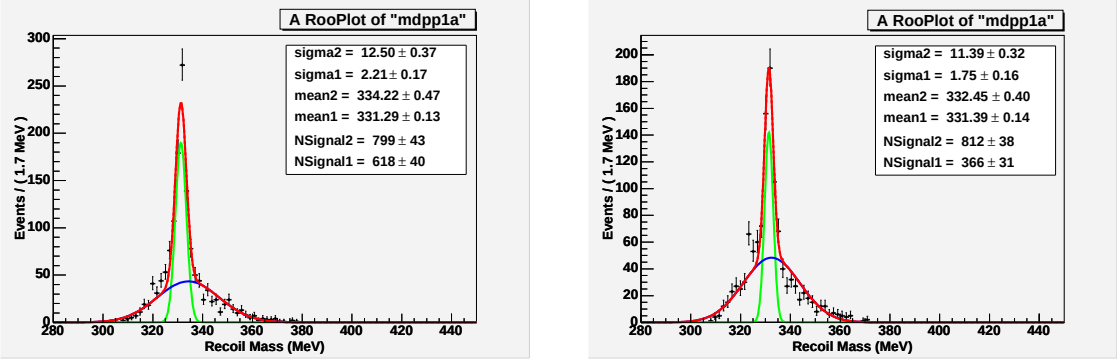

Figure 6.2: Double-Gaussian fits to the muon (left) and electron (right) "existence" Monte Carlo events, using the additional soft cuts listed above.

We then apply this same fitting procedure to data events, again separately for muon and electron final states. With the additional soft cuts, the electron channel is now much cleaner and we are actually able to perform a double-Gaussian fit. We use the same parameters found from the Monte Carlo events - the separation of the two gaussian means, the relative areas, and the fitted sigma values - though we allow the mean of the narrow Gaussian and the total area to vary accordingly. Background - either QED or otherwise - is fitted to a third Gaussian shape. The moun and electron events from data are shown in Figure 6.3.

Table 6.1 shows the results of the fitting procedure in data. We measure 154 ± 13 $\mu^+\mu^-$ "existence" events and 152 ± 39 e^+e^- "existence" events. Comparing the sum of these two to the number of total "existence" events expected in data, we measure an *observed* efficiency of $(4.8 \pm 0.8)\%$. This is to be compared to the overall efficiencies predicted from Monte Carlo, given above.

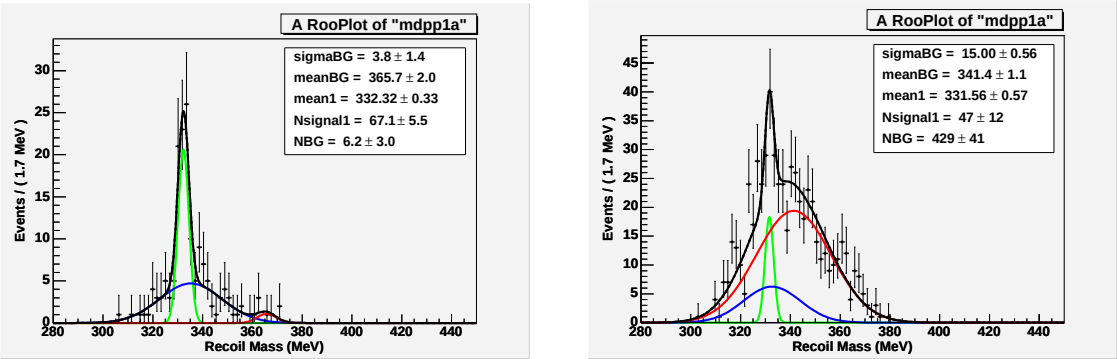

Figure 6.3: Double-Gaussian fits to the muon (left) and electron (right) "existence" data events. The new soft cuts greatly reduce the QED background initially seen in the electron channel.

While the error on the observed efficiency allows us only to demonstrate these numbers agree to within $0.8/4.8 = 16\%$, this is still a significant triumph. We assign no systematic uncertainty on our Monte Carlo efficiencies at this time. (These will be discussed more thoroughly in Chapter 8.)

Table 6.1: Roofit fitting parameters for muon and electron events in both Monte Carlo and data. We fix the overall shapes and relative sizes in Monte Carlo, then apply these parameters to the "existence" events seen in data. The overall mean and total area are allowed to float.

	Monte Carlo		Data	
Parameter	$\mu^+\mu^-$	e^+e^-	$\mu^+\mu^-$	e^+e^-
$\bar{x}_{narrow}$(MeV)	331.3	331.4	332.3	331.6
$\bar{x}_{wide} - \bar{x}_{narrow}$ (MeV)	2.9	1.1	fixed	fixed
Total Area	1417	1178	153.9	151.3
$\text{Area}_{wide}/\text{Area}_{narrow}$	1.29	2.22	fixed	fixed
σ_{narrow} (MeV)	2.2	12.5	fixed	fixed
σ_{wide} (MeV)	1.8	11.4	fixed	fixed

6.2 Efficiency and $\chi^2_{\gamma\gamma}$ Check for the Single Pion Analysis

We perform a similar check for the single pion analysis. Here we make use of the well-known "Tomasz" channel, the main background to our signal process. This decay channel has $\Upsilon(3S) \rightarrow \pi^+\pi^-\Upsilon(2S) \rightarrow \pi^+\pi^-\gamma_1\chi_b \rightarrow \pi^+\pi^-\gamma_1\gamma_2\Upsilon(1S)$, with $\Upsilon(1S) \rightarrow \ell^+\ell^-$. From evaluating the number of background events falling into the "Tomasz" measurement region in the single pion analysis, we observe that this channel will be relatively background-free. Since we here change our photon energy sum to fit the "Tomasz" transition instead of our signal process (550 MeV, instead of 518.3 MeV), potential background should be even less likely.

We apply the same post-processor cuts used in our single pion analysis, changing only the bounds of our measurement region to capture the new distribution of the missing pion mass. The distributions from "Tomasz" Monte Carlo, shown in Figure 6.4, give an overall efficiency of $(12.7 \pm 0.2)\%$. This gives an expected signal size of 41 ± 12 events in $\Upsilon(3S)$ data. For comparison, we also show the Monte Carlo distribution of $\chi^2_{\gamma\gamma}$ for the "Tomasz" events.

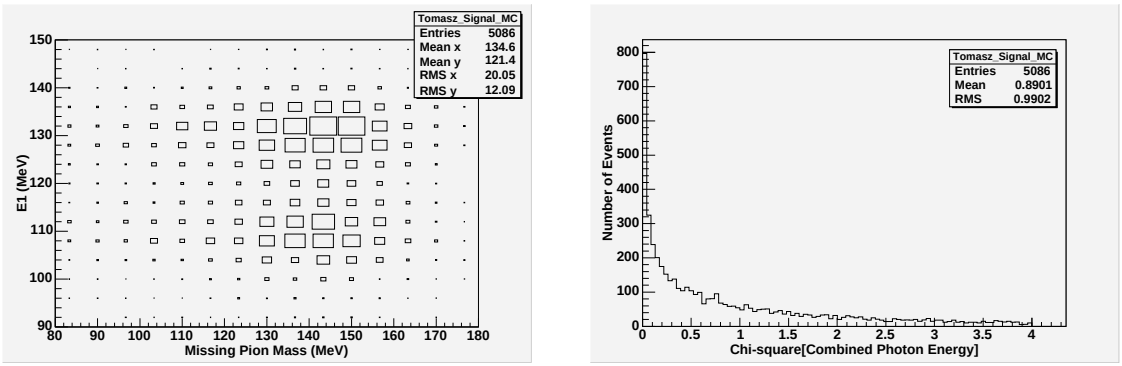

Figure 6.4: The signal event (left) and $\chi^2_{\gamma\gamma}$ distributions from "Tomasz" Monte Carlo for the single pion analysis check.

Results from running our processor over the $\Upsilon(3S)$ data are shown in Figure 6.5. We see 49 events in our measurement region, entirely consistent with our prediction

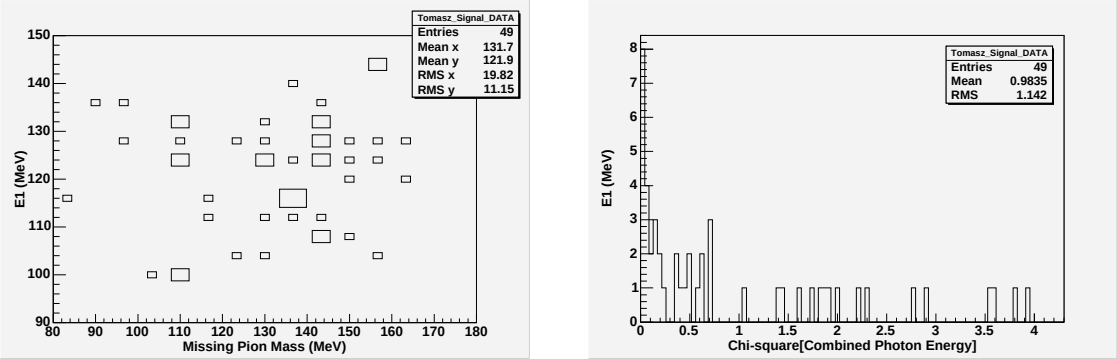

Figure 6.5: The signal event (left) and $\chi^2_{\gamma\gamma}$ distributions from "Tomasz" *data* for the single pion analysis check.

Table 6.2: Distribution of $\chi^2_{\gamma\gamma}$ in both Monte Carlo and data events, for our "Tomasz" check of the single pion analysis.

$\chi^2_{\gamma\gamma}$ bin	MC fraction	Data fraction
$0 \rightarrow 1$	67	65 ± 11
$1 \rightarrow 2$	18	18 ± 6
$2 \rightarrow 3$	9	8 ± 4
$3 \rightarrow 4$	6	8 ± 4

of 41 ± 12 events. We attribute, at this point, no systematic uncertainty to the overall efficiencies in our single pion analysis.

We also wish to demonstrate that the distribution of $\chi^2_{\gamma\gamma}$ - the fit of γ_1 and γ_2 to a fixed photon energy sum - is consistent between "Tomasz" Monte Carlo and data. The corresponding results are shown in Table 6.2. We had established an upper limit cut at $\chi^2_{\gamma\gamma} < 4$, and bin the remaining values in increments of one. As shown, the distributions between events in Monte Carlo and data are quite consistent.

From this, we can feel confident that the photon-fitting code within our processor is working properly. In the next section, having checked the results of our processor for both analyses, we present our results from Υ(3S) data.

CHAPTER 7

RESULTS FROM DATA

We run our processor over the $(5.81 \pm 0.12) \cdot 10^6$ $\Upsilon(3S)$ events in CLEO datasets `data16`, `data17`, and `data22`. The events falling into each of our three measurement regions for both the di-pion and single pion analyses are shown in Figure 7.1.

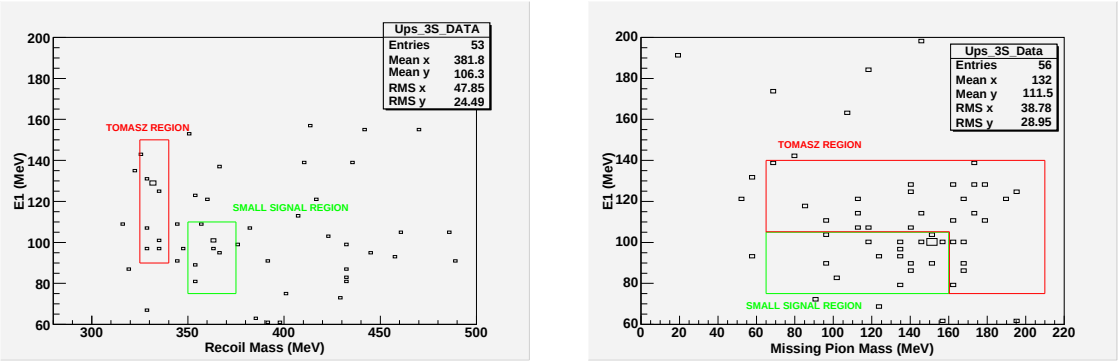

Figure 7.1: Distribution of events from *data* falling into our three measurement regions, for both the di-pion (left) and single pion (right) analyses.

7.1 Di-pion Analysis Results

Table 7.1 shows the summed expected background for each measurement region in the di-pion analysis, as well as the number of events actually seen in data (from the left half of Figure 7.1).

We see 36 events falling into the "Sideband" measurement region, to be compared with our expected background of 22.7 ± 4.4 events. This result is approximately a 1.8σ overall deviation (taking into account the Poisson error on the number of observed events), although separating the events into muon and electron final states is perhaps more revealing. Here, the $\ell = \mu$ events are consistent in number with the expected value, while the electron events show a significant

excess. As seen in the di-pion analysis check in the previous chapter, this QED background in the electron channel is perhaps to be expected, though we tried to eliminate some of it with our additional soft cuts to the pion and lepton tracks. Later in this section we will scale this excess background into the other two measurement regions to get a more conservative background estimate.

Table 7.1: Data results for the *di-pion* analysis. The background estimate in each measurement region is the sum, with uncertainty, from the previous tables.

Region	Υ(1S)$\rightarrow$	Est. Occupancy [Tab. 5.1]	N_{obs}
Sideband	$\ell\ell$	22.7 ± 4.4	36
"Tomasz"	$\ell\ell$	8.6 ± 2.0	10
Signal	$\ell\ell$	0.6 ± 0.2	7
Sideband	$\mu\mu$	12.2 ± 3.1	11
"Tomasz"	$\mu\mu$	4.9 ± 1.2	6
Signal	$\mu\mu$	0.4 ± 0.2	6
Sideband	ee	10.4 ± 2.9	25
"Tomasz"	ee	3.9 ± 0.9	4
Signal	ee	0.4 ± 0.2	1

In the "Tomasz" measurement region, we see good agreement between the number of events predicted by Monte Carlo (8.6 ± 2.0) and the number of events actually seen (10). The separated muon and electron final states are in good agreement as well.

Finally, we expect 0.6 ± 0.2 background events in the "Signal" region and instead see 7 events. To evaluate the null hypothesis - i.e., how well the expected background levels can account for the excess events seen in data - we evaluate the Poisson probability that $0.6 + 1.28 \cdot 0.2 = 0.86$ events can fluctuate up to seven of more. (Here our background estimate takes the mean value plus an additional contribution from the error, using a 90% one-sided Gaussian limit). This corresponds to a Poisson probability of 3.3×10^{-5}, or a 4.0σ one-sided Gaussian deviation.

As this is greater than 3σ, we are able to claim "evidence" of our signal process, $\chi_b' \to \chi_b\ \pi^+\pi^-$. The event display for one of our likely signal events is shown in Figure 7.2.

Alternatively, one can use the excess events falling into the large "Sideband" region to predict the amount of additional background that can be expected in the other two regions. We do this to arrive at a more conservative estimate of any potential signal, by effectively smearing excess events seen in the large region into the background expectations for the two smaller regions. Taking these 36 "Sideband" data events and subtracting away the 22.7 ± 4.4 events that we actually expect to see here, we see an excess of 13.3 ± 7.4 events (having assigned a Poisson error to the number of observed data events). We then scale this excess into each of the other two regions, multiplying by the ratios of the region areas. For example, our "Tomasz" region is allocated $(13.3 \pm 7.4) \cdot (900 MeV^2)/(29025 MeV^2) = 0.4 \pm 0.2$ events, plus the 8.6 ± 2.0 events expected from our considerations of all the known backgrounds. These new background values are compiled in Table 7.2.

Table 7.2: Similar to the previous table for the *di-pion* analysis, but with the estimated background now including a scaled contribution from excess data events seen in the "Sideband" region.

Region	Υ(1S)$\to$	Est. Occupancy	N_{obs}
Sideband	$\ell\ell$	36.0 ± 6.0	36
"Tomasz"	$\ell\ell$	9.0 ± 2.0	10
Signal	$\ell\ell$	1.0 ± 0.3	7

The Poisson probability of this new background prediction for our "Signal" region (*i.e.,* $1.0 + 1.28 \cdot 0.3 = 1.38$) fluctuating up to seven or more events is 5.7×10^{-4}, which corresponds to 3.3σ for a Gaussian distribution. Again, even this conservative estimate for the signal size gives "evidence" of the χ_b' decay.

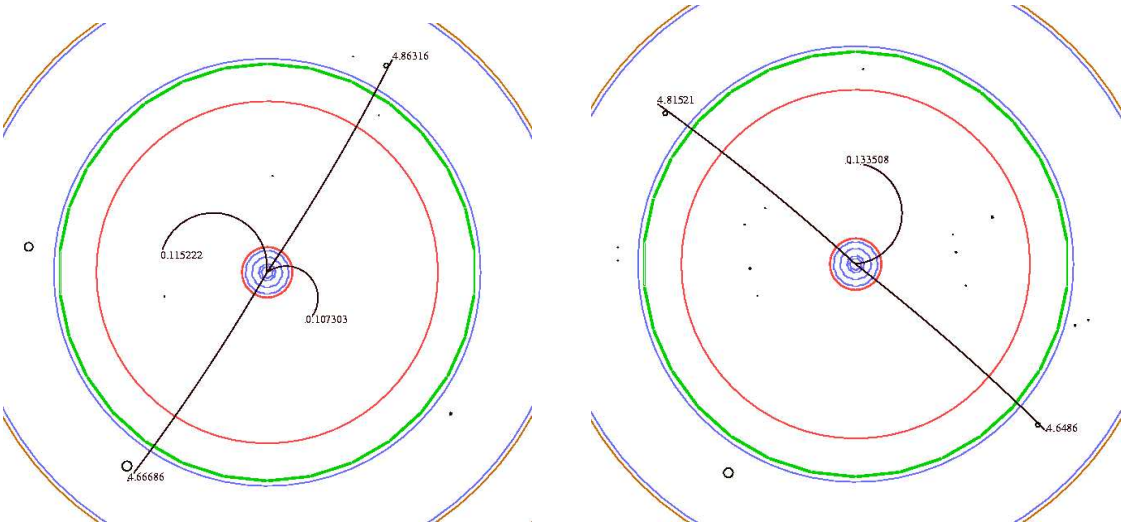

Figure 7.2: Event displays showing likely signal events for both the di-pion (left) and single pion analyses.

Galik also does a third calculation for estimating the likelihood that the background can account for the observed signal size. Assuming the background distribution to be Gaussian, with a mean of 1.0 and width of 0.3, he throws a sizable number of background values with this distribution and determines what likelihood these values have of being greater than or equal to seven. He calculates a probability of 2.2×10^{-4}, corresponding to a 3.5σ effect.

Finally, of slight concern was the fact that we see six muon events and only one electron event in our "Signal" region. One possibility is that unaccounted-for noise photons in the *ee* events would lower the efficiency of this channel. Assuming that this is not the case, and that muon and electron events are equally likely, Galik calculates a probability-maximizing mean of 3.8 events per channel, with an overall probability of about 2% for this value fluctuating to the observed values.

7.2 Single Pion Analysis Results

The data events falling into our three measurement regions for the single pion analysis are shown in the right half of Fig. 7.1. The summed contributions from known backgrounds (Table 5.2) are again put alongside the number of *observed* data events we see in each region, in Table 7.3.

Table 7.3: Data results for the *single pion* analysis. The background estimate in each measurement region is the sum, with uncertainty, from the previous tables.

Region	$\Upsilon(1S)\rightarrow$	Est. Occupancy [Tab. 5.2]	N_{obs}
Large	$\ell\ell$	5.3 ± 1.4	13
"Tomasz"	$\ell\ell$	17.2 ± 4.8	26
Signal	$\ell\ell$	2.2 ± 0.6	17
Large	$\mu\mu$	2.5 ± 0.6	5
"Tomasz"	$\mu\mu$	9.0 ± 2.6	12
Signal	$\mu\mu$	1.1 ± 0.3	9
Large	ee	2.8 ± 1.0	8
"Tomasz"	ee	8.1 ± 2.2	14
Signal	ee	1.1 ± 0.3	8

In the "Sideband" region, we see 13 events in data, having predicted 5.3 ± 1.4. (Note that five of these events have $m_{\pi\pi}$ values outside the physically-allowed region, and could be removed with a soft cut on this variable. See Section 7.4.) Both the separated $\ell = \mu$ and $\ell = e$ analyses indicate a slight excess of events in this measurement region, though there is a more pronounced deviation in the latter case. This can perhaps be attributed to QED backgrounds that have managed to pass our processor requirements. We will again scale these excess data events into both the "Tomasz" and "Signal" regions.

As in the di-pion analysis, the expected number of events in the "Tomasz" region is consistent with what we observe in data. 17.2 ± 4.8 events are predicted

in this region from known backgrounds, and we see 26 data events. Both electron and muon events are within 3σ of the expected values.

Again our main region of interest is the "Signal" region, where we expect the majority of our signal events to fall. Known backgrounds predict 2.2 ± 0.6 events in our signal region, but we see 17 events when looking at data - a strong indication of our decay process. (9 of these likely signal events are $\ell = \mu$ events; 8 are $\ell = e$ events.) Even upon taking the excess data events seen in the "Sideband" region and scaling that excess into our "Signal" region (again, by the ratio of their areas), we still expect only 3.2 ± 0.8 events. These scaled values are summarized in Table 7.4.

Table 7.4: Similar to the previous table for the *single pion* analysis, but with the estimated background now including a scaled contribution from excess data events seen in the "Sideband" region.

Region	$\Upsilon(1S) \rightarrow$	Est. Occupancy	N_{obs}
Large	$\ell\ell$	13.0 ± 3.6	13
"Tomasz"	$\ell\ell$	19.6 ± 4.9	26
Signal	$\ell\ell$	3.2 ± 0.8	17

We follow the same line of reasoning taken with the previous di-pion analysis, calculating the Poisson probability that either 2.2 ± 0.6 events or 3.2 ± 0.8 events (our more conservative approach) can fluctuate enough to account for the 17 events we see in data. In the first case, again taking a 90% one-sided Gaussian limit for the estimate of the background, the Poisson probability that $2.2 + 1.28 \cdot 0.6 = 2.97$ events can account for our signal is 1.9×10^{-8}, corresponding to 5.5σ. The Poisson probability for the latter, more conservative estimate of background events gives 2.3×10^{-6}, corresponding to 4.6σ. For the third approach, we again assume a Gaussian distribution for the expected background, with central value of 3.2 and

a width of 0.8. This gives a probability of 1.4×10^{-6} for the null hypothesis, corresponding to 4.7σ. In all three cases we can confidently refute the null hypothesis: that background could account for the observed signal. This is the same result we came to in the di-pion analysis, and we again find clear "evidence" for the χ_b' decay.

We will combine the Poisson probability results for both the di-pion and single pion analyses in the next section.

Staying with the single pion analysis for the moment, it should be noted that our processor also keeps track of the "best pi0 pull" for all of the passing events - a measure of the best likelihood that any two photons in that event reconstruct to a π^0. Of the data events passing our processor (without cuts), we see a sizable peak for this variable near zero. This would tend to indicate the presence of some prominent π^0 or η background. However, once we apply all of our cuts to the data events passing our processor, very few likely π^0 candidates appear in our 2-D measurement regions. In our "Signal" region, there is only one event with a likely "pi0 pull" (of $\sim$1). We make no subtraction for this event, but simply verify that we have little, if any, π^0 or η background in our "Signal" region.

As an additional check, we look at the distribution of $\chi^2_{\gamma\gamma}$ for the events falling into our three measurement regions. From Monte Carlo, this variable peaks strongly for our signal process, less strongly for the "Tomasz" process, and not much at all for the other likely backgrounds. In Figure 7.3, we again show the measurement regions for our single-pion analysis, but this time we have coded the event markers according to their value of $\chi^2_{\gamma\gamma}$. Black markers indicate events with $\chi^2_{\gamma\gamma}$ values between 0 and 1; light grey between 1 and 2; solid lines between 2 and 3; and dotted lines indicate events with $\chi^2_{\gamma\gamma}$ values between 3 and 4. Most of the

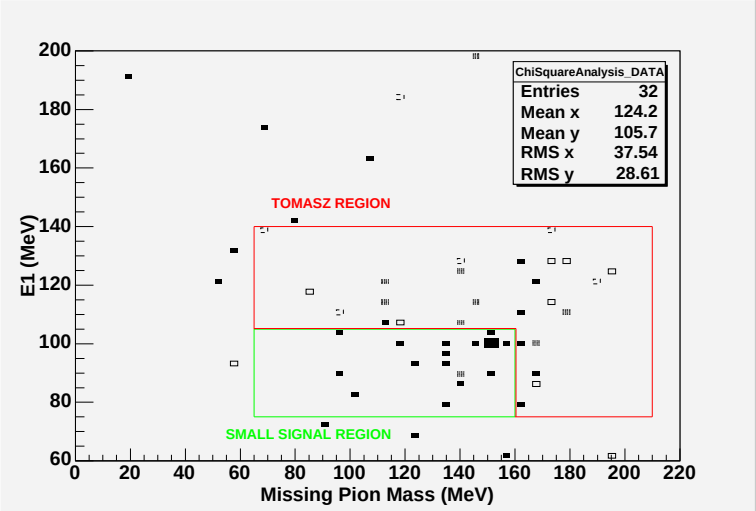

Figure 7.3: The events falling into our three measurement regions for the *single pion* analysis are shown above, color-coded by their $\chi^2_{\gamma\gamma}$ value.

events in the "Signal" region show very low values for $\chi^2_{\gamma\gamma}$, indicating excellent fits to our signal's photon energy sum. The distribution is consistent with the expectation from Monte Carlo.

7.3 Final Refutation of the Null Hypothesis

Having established these final checks for our single pion analysis, we go forward and combine the Poisson probability considerations for both the di-pion and single pion analyses, producing a coordinated refutation of the null hypothesis. The results of this are summarized in Table 7.5.

As previously indicated, there are two ways to calculate these values, the latter of which takes into account potentially-excess background in the "Sideband" region of our analysis and scales this background into our "Signal" region. In both ways of estimating the background, however, we can (by combining our results from both the di-pion and single pion analyses) confidently state that we indeed have

an *observation* of the χ_b' decay process.

In the following subsections, we go forward to show the invariant mass of the di-pion system for our likely signal events, as well as extracting a value for the partial width of our observed decay.

Table 7.5: A summary of results from both the di-pion and single pion analyses, in which the Poisson probabilities (that the expected background could account for the observed signal) are shown. Corresponding values for a Gaussian probability distribution are included. We here combined the results from both analyses, coming to a final refutation of our null hypothesis.

Background Expectation	Analysis	Poisson Probability	Gaussian Deviation
Regular	Di-Pion	$3.3 \cdot 10^{-5}$	4.0σ
(from Monte Carlo estimates)	Single Pion	$1.9 \cdot 10^{-8}$	5.5σ
$\overline{b} + 1.28\sigma$	Combined	$6.2 \cdot 10^{-13}$	$\mathbf{7.1}\sigma$
Conservative	Di-Pion	$5.7 \cdot 10^{-4}$	3.3σ
(w/ scaled sideband)	Single Pion	$2.3 \cdot 10^{-6}$	4.6σ
$\overline{b} + 1.28\sigma$	Combined	$1.3 \cdot 10^{-9}$	$\mathbf{6.0}\sigma$
Conservative	Di-Pion	$2.2 \cdot 10^{-4}$	3.5σ
(w/ scaled sideband)	Single Pion	$1.4 \cdot 10^{-6}$	4.7σ
Distribution of mean bckgnd	Combined	$3.0 \cdot 10^{-10}$	$\mathbf{6.2}\sigma$

7.4 Di-Pion Mass Distributions

Between our di-pion and single pion analyses, we have a total of approximately 24 likely signal events (two or three of which are likely to come from background processes). In spite of limited statistics, we here present the di-pion mass distribution for those data events falling into our "Signal" regions.

For the di-pion analysis, in which we see both soft pion tracks, the di-pion mass is calculated simply as the invariant mass of the sum of the two pion 4-vectors:

$$m_{\pi\pi} = \sqrt{(\mathcal{P}_+ + \mathcal{P}_-)^2} \ . \tag{7.1}$$

In the single pion analysis, however, this 4-vector sum is carried out by using the available 4-vectors from the beam energy and the other observed particles. Using notation consistent with our previous missing pion reconstruction, we calculate the di-pion invariant mass from the single pion analysis to be:

$$m_{\pi(\pi)} = \sqrt{(\mathcal{P}_\pi + \mathcal{P}_{miss})^2} = \sqrt{(\mathcal{P}_{bm} - \mathcal{P}_\Upsilon - \mathcal{P}_{\gamma 1}^{fit} - \mathcal{P}_{\gamma 2}^{fit})^2}\ . \tag{7.2}$$

The results from the di-pion and single pion analyses are shown in Figure 7.4, both separately (left) and combined (right).

Two of the events from the single pion analysis fall below the lower limit of this plot (the dotted line indicates $2m_\pi$, the minimum physically-allowed value). This occurs as a consequence of the spreading of measurements in the reconstruction process, and 6% of the signal Monte Carlo events in the single pion analysis also fall below this point (corresponding to $\sim$1 expected data event). The upper limit of the di-pion invariant mass is dependent upon the J value of the $\chi_b' \rightarrow \chi_b\ \pi^+\pi^-$ transition.

From the plots below, our di-pion invariant mass plot seems to suggest a high-mass Yan distribution, although the statistics here are terribly limited. For comparison, we also show a plot of the $m_{\pi\pi}$ distribution for those events falling into the "Sideband" and "Tomasz" measurement regions in the single pion analysis. 19 of these events are expected to be from the "Tomasz" process, and here we see a prominent high-mass peak as expected. Additionally, we see five "Sideband" events which fall well outside the physically-allowed region of $m_{\pi\pi}$. In hindsight, one could have applied a 100%-efficient cut to this variable that would have significantly decreased the excess number of events seen in the "Sideband" region.

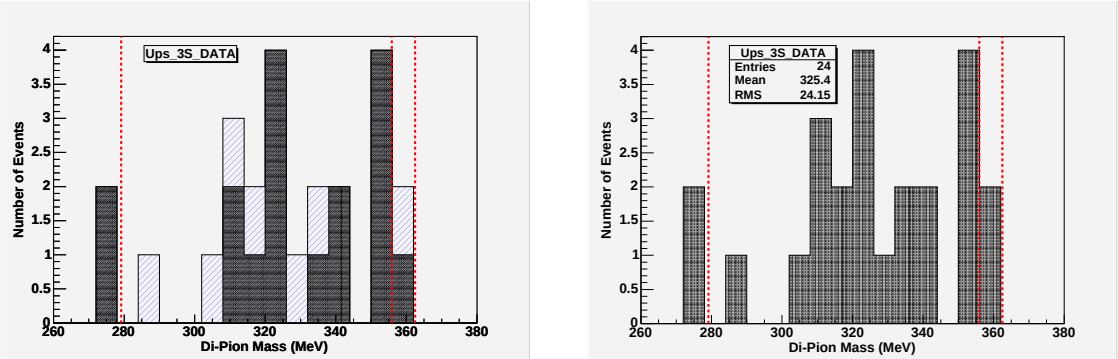

Figure 7.4: Di-pion invariant mass distributions for likely signal events in both the di-pion and single pion analyses. Shown separately on the left, these twenty-four events are combined in the righthand figure.

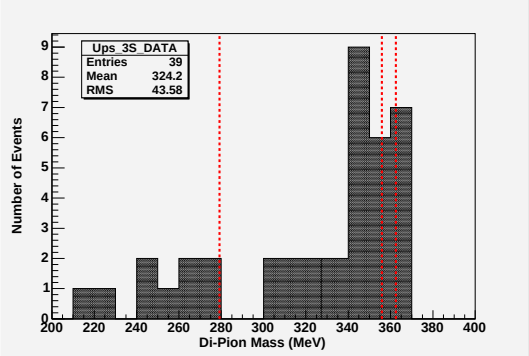

Figure 7.5: Di-pion invariant mass distributions for events in the "Sideband" and "Tomasz" regions of the single pion analysis.

7.5 Partial Width Calculations

Using the yield of events in the "Signal" region from our single pion analysis, we can extract a partial width value for our decay process. Because we can't easily separate the 1-to-1 and 2-to-2 signal events in this analysis, we rely upon a few simple assumptions to extract an overall partial width.

We assume first that there is no D-wave component to this transition (arguments to this effect were assessed in Section 2.2), such that the 0-to-0, 1-to-1, and 2-to-2 decays are all equally probable. Further, we note that the small overall branching fraction for 0-to-0 events discriminates against any of these decays appearing in our "Signal" region, as well as the fact that its γ_1 transition should fall outside the bounds of our assessed cuts. Thus, the 0-to-0 contribution is assumed to be negligible and the partial widths for 1-to-1 and 2-to-2 events will be approximately equal. We can then solve for this term, $\Gamma_{\pi^+\pi^-}$.

The number of Υ(3S) events times the summed overall branching fractions of the two channels is then equal to the number of observed events, as follows:

$$N_{sig} = N_{3S} \cdot \mathcal{B}_{\Upsilon\ell^+\ell^-} \cdot \Gamma_{\pi^+\pi^-} \cdot [\quad \mathcal{B}_{\gamma 1,1}\ \epsilon_{1\to 1}\ \mathcal{B}_{1,\gamma 2}/\Gamma_{tot}(\chi'_{b1}) + \mathcal{B}_{\gamma 1,2}\ \epsilon_{2\to 2}\ \mathcal{B}_{2,\gamma 2}/\Gamma_{tot}(\chi'_{b2}) \ ] \tag{7.3}$$

where the E1 transition notations are reasonably clear and were introduced previously, and $N_{sig} = N_{obs} - N_{bkg}$. For our estimate of the expected background we use the weighted average of the background expected in Monte Carlo (Table 7.3) and the background that uses a rescaling of the events in the "Sideband" region (Table 7.4); this gives $N_{bkg} = 2.6 \pm 0.5$, where 0.5 is half the difference between the two background estimates. Thus, $N_{sig} = 17 - 2.6 = 14.4$. The statistical error on this value will simply be the square-root of N_{sig}, and the systematic error will come

entirely from the estimated error in N_{bkg} (namely, 0.5). All of the $\mathcal{B}$ have been used previously in this paper, and $N_{3S} = (5.81 \pm 0.12) \times 10^6$. The overall efficiency for each transition is calculated as the weighted average of the efficiency values measured from `data16` and `data22` signal Monte Carlo samples, taking into account differences in photon energy resolutions and summarized in Eqn. 4.9. Finally, the two total widths, $\Gamma_{tot}(\chi'_{b1}) = (96 \pm 16)$ keV and $\Gamma_{tot}(\chi'_{b2}) = (138 \pm 19)$ keV, were calculated within our CBX note[1] from the experimental branching fractions and theoretical partial widths for E1 transitions of the χ'_{bJ}.

The only statistical uncertainty comes from N_{sig}. From these values we obtain (showing only the *statistical* uncertainty), from the single-pion analysis:

$$\begin{aligned}(14.4) = (5.81 \cdot 10^6) \cdot 4.96\% \cdot \Gamma_{\pi^+\pi^-} \cdot [\quad & 11.3\% \cdot 10.8\% \cdot 35\%/(96\text{keV}) \\ + \quad & 11.4\% \cdot 9.7\% \cdot 22\%/(138\text{keV}) \ ] \end{aligned} \quad (7.4)$$

This evaluates to:

$$\Gamma_{\pi^+\pi^-} = (0.80 \pm 0.21) \text{ keV} \ . \quad (7.5)$$

7.6 Systematic Errors

The only physical quantity that we actually measure in this analysis is the partial width of our signal decay processes. A statistical error for this value (arising from the square root of the number of observed events) was presented in the previous section.

The general process for determining the systematic error on a value computed from a slightly complex formula, with each term contributing some systematic error of its own, is to generate an overall distribution of this quantity using a toy Monte Carlo sample. The value is calculated a large number of times (for us, a

million times) with each variable individually being thrown as a Gaussian with the associated mean and standard deviation. From the distribution of $\Gamma_{\pi^+\pi^-}$ that results (which will be asymmetric), we can assess appropriate bounds and extract the overall systematic errors.

The first step is to assess the systematic errors of each individual term. Most of the values in Equation 7.3, specifically the branching fractions, get their systematic errors from the Particle Data Group[4] values. The systematic error on N_{sig} comes from the error on N_{bkg}, and is taken to be half the difference between our two background expectations (regular and conservative) in the single pion analysis. Thus, N_{sig} is thrown as 14.4 ± 0.5. The full widths of the χ_b' states arise from Galik's calculation within our CBX note: $\Gamma_{tot}(\chi_{b1}') = (96 \pm 16)$ keV and $\Gamma_{tot}(\chi_{b2}')$ $= (138 \pm 19)$ keV.

The main difficulty comes from assessing the systematic errors on the overall efficiencies for our 1-to-1 and 2-to-2 signal processes. There will be both a correlated error - such that we throw a Gaussian distribution of mean 1 with appropriate sigma, and multiply this to both efficiency terms - and an uncorrelated error. The correlated error arises from systematic errors specific to the CLEO detector and from different possible $m_{\pi\pi}$ distributions. The uncorrelated error arises from differences in how well the overall efficiencies vary between datasets and how they are altered by proposed changes to the γ_1 energy distributions. All of these systematic error contributions are assembled in Table 7.6 below.

Taking these contributing terms in quadrature, we estimate our 1-to-1 and 2-to-2 overall efficiencies as:

$$\epsilon_{1\to1} = (1 \pm 0.07) \times (10.8 \pm 0.8)\% \tag{7.6}$$

$$\epsilon_{2\to2} = (1 \pm 0.07) \times (9.7 \pm 0.3)\% \tag{7.7}$$

Table 7.6: Compilation of systematic uncertainties to the overall efficiencies in the single pion analysis. Correlated uncertainties are given as relative percentages, while the individual uncertainties are given as absolute values, in percent.

Source	Corr Uncert	Uncert in $\epsilon_{1\to1}$	Uncert in $\epsilon_{2\to2}$
Limited MC statistics	-	0.3	0.3
`data16-22` difference	-	0.5	negl
Peak Photon Energy	-	0.1	negl
Width of Photon Energy	-	0.5	0.1
Shape of $m_{\pi\pi}$ distribution	2	-	-
Decay ang. distributions	2	-	-
Track-finding probab.	6	-	-
Photon-finding probab.	2	-	-
$\ell = e/\mu$	1	-	-
Other selection criteria	-	negl	negl
Sum	7%	0.8	0.3

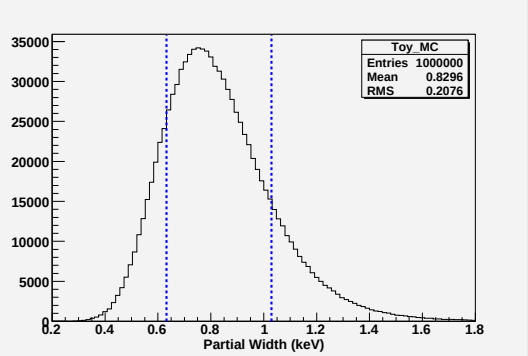

Figure 7.6: Toy Monte Carlo distribution for determining the systematic errors on the partial width. Boundaries symmetrically surrounding 68.3% of the values are indicated by the dotted lines.

The toy Monte Carlo then throws all of these variables in accordance with their Gaussian distributions, calculating the resultant $\Gamma_{\pi^+\pi^-}$ each time. The generated distribution, throwing 10^6 events, is shown in Figure 7.6. To extract the systematic uncertainties, we determine the upper and lower values of $\Gamma_{\pi^+\pi^-}$ that symmetrically bound 68.3% of the values, and then subtract each of these limits from the mean

value of the partial width. Putting these determined values with the statistical error from the previous section, we determine a final partial width value for our 1-to-1 and 2-to-2 $\chi_b' \to \chi_b\ \pi^+\pi^-$ decays of:

$$\Gamma_{\pi^+\pi^-} = (0.80\ \pm 0.21\ \pm^{0.23}_{0.17})\ \text{keV}\ . \tag{7.8}$$

CHAPTER 8

CONCLUSION

This work is the culmination of two summers and an academic year spent at Wilson Laboratory as part of the CLEO Collaboration, working through the graduate physics program at Cornell University. The research was first suggested by Rich Galik and is a continuation of an initial inquiry conducted by Tatia Engelmore[1], then an undergraduate student at Cornell.

We here used the wealth of CLEO-III $\Upsilon(3S)$ data to look for a rather rare decay in the $b\bar{b}$ system, confining our research to the two most likely transitions between the χ_b' and χ_b triplet states. We found evidence of a signal in both our di-pion and single pion analyses, and were able to claim a first observation by combining these two results. We also presented the di-pion mass spectrum for our likely signal events and, making a few reasonable assumptions, extracted a partial width for these decay processes of $\Gamma_{\pi^+\pi^-} = (0.80 \ \pm 0.21 \ \pm \ ^{0.23}_{0.17})$ keV.. We have checked our event processor using known decay channels to verify that it is, in fact, doing what we should like it to do.

Currently, we are extending this research to include the neutral channel, $\chi_b' \rightarrow \chi_b\pi^0\pi^0$. Because the charged and neutral channels should present similar results to one another (the neutral channel likely exhibiting about half the branching fraction), verification that we indeed see this neutral channel will only further strengthen our case for observation of the charged transition.

[1]CU Class of 2004, presently at Columbia Univ. Physics

APPENDIX A

THE *RADLEP* SUBCOLLECTION

In this analysis we use the *radlep* subcollection in the event database. For reference, the *radlep* subcollection for datasets 16 and 17 [1] is made up of events which pass the union of

1. radBhha: $nTk > 1 \oplus pTk1 > 0.4 \oplus eOverP1 > 0.5 \oplus eGam1 > 0.02 \oplus eVis > 0.75 \oplus acop > 0.01$

2. radMuP $1 < nTk < 4 \oplus pTk1 > 0.4 \oplus eOverP1 < 0.85 \oplus eOverP2 < 0.85 \oplus eGam1 > 0.02 \oplus eVis > 0.75$

3. muPair $nTk > 1 \oplus pTk2 > 0.4 \oplus eOverP1 < 0.85 \oplus eOverP2 < 0.85$

4. radGam $nTk < 2 \oplus eSh2 > 0.4 \oplus eSh3 > 0.08 \oplus eCC > 0.75$

5. loPt2Leptons $loPtTwoTk \oplus pTk1 > 0.06 \oplus acop < 0.05$

6. loPt4Pions $loPtGT2Tk \oplus pTk1 > 0.02 \oplus nTk = 4 \oplus qNet = 0$

7. tranLep $tranDiMuon$ OR $tranDiElec$ OR $tranLepTk$

Quantities used above are:[2]

- qNet = net charge of tracks in event
- nTk = number of charged tracks in event
- pTk1 = largest track momentum in event

[1] Data subcollections are subject to change from dataset to dataset, and what we describe here is the definition specifically valid for datasets 16 and 17.

[2] All momenta and energies are defined as ratios to E_{beam}, unless otherwise noted.

- pTk2 = second largest track momentum in event
- eTk1 = matched calorimeter energy for pTk1
- eTk2 = matched calorimeter energy for pTk2
- eSh1 = energy of most energetic shower in event to E_{beam}
- eSh2 = energy of second most energetic shower in event to E_{beam}
- eSh3 = energy of third most energetic shower in event to E_{beam}
- eCC = calorimeter energy / (2^*E_{beam})
- eNeu = part of eCC not matched to tracks
- eChg = assuming pion hypothesis, sum of all track energies in event / (2^*E_{beam})
- eVis = eNeu + eChg
- eOverP1 = eTk1/pTk1
- eOverP2 = eTk2/pTk2
- eGam1 = energy of largest unmatched shower
- ϕ_1 = angle ϕ for highest momentum track
- ϕ_2 = angle ϕ for second highest momentum track
- acop = $|\pi - |\phi_1 - \phi_2||$
- loPtTwoTk = $eVis < 0.75 \ \oplus \ eVis > 0.04 \ \oplus \ nTk = 2 \ \oplus \ qNet = 0$
- loPtGT2Tk = $eVis < 0.75 \ \oplus \ eVis > 0.04 \ \oplus \ nTk > 2$

- tranDiMuon = $eMiss \ \oplus \ eGam1 > 0.02 \ \oplus \ eNeu > 0.02 \ \oplus \ diMuon$
- tranDiElec = $eMiss \oplus eGam1 > 0.03 \oplus eNeu > 0.02 \oplus diElec \oplus eChg < 1$
- tranLepTk = $nTk > 3 \ \oplus \ eMiss \ \oplus \ (diMuon \ \text{OR} \ diElec)$
- eMiss = $nTk > 1 \ \oplus \ pTk2 > 0.5 \ \oplus \ eVis - sum12 > 0.02$
- diMuon = $eTk1 < 1/eBeam \ \oplus \ eTk2 < 1/eBeam$
- diElec = $eOverP1 > 0.5 \ \oplus \ eOverP2 > 0.5$

REFERENCES

[1] T.K. Engelmore, R.S. Galik (Cornell University, Laboratory for Elementary-Particle Physics), and K.M. Weaver, (CLEO Collaboration Internal Note). "Observation of $\chi_b' \rightarrow \chi_b \pi^+\pi^-$." CBX 05-19 (2005): 1-55. Contact Rich Galik with further inquiries.

[2] T. M. Yan. "Hadronic transitions between heavy-quark states in quantum chromodynamics." Physical Review D 22 (1980): 1652-68.

[3] W. Kwong, J.L. Rosner, and C. Quigg. "Heavy-Quark Systems." Ann. Rev. Nucl. Part. Sci. 37 (1987): 325-82.

[4] S. Eidelman *et al.*, (Particle Data Group). "Review of Particle Physics." Physics Letters B 592 (2004): 1-1109.

[5] D. Cronin-Hennessy *et al.*, (CLEO Collaboration). "Observation of the Hadronic Transitions $\chi_{b1,2}(2P) \rightarrow \omega\Upsilon(1S)$." Physical Review Letters 92 (2004): 222002.

[6] J.J. Aubert *et al.* "Experimental Observation of a Heavy Particle J." Physical Review Letters 33 (1974): 1404-6.

[7] J.E. Augustin *et al.* "Discovery of a Narrow Resonance in e^+e^- Annihilation." Physical Review Letters 33 (1974): 1406-8.

[8] J.P. Alexander *et al.*, (CLEO Collaboration). "Hadronic transitions $\Upsilon(2S) \rightarrow \Upsilon(1S)$." Physical Review D 58 (2004): 052004.

[9] G. Abrams. Proceedings of the 1975 International Symposium on Lepton and Photon Interactions at High Energies. Stanford Linear Accelerator Center, Menlo Park, CA. 1975.

[10] J.Z. Bai *et al.*, (BES Collaboration). "$\psi(2S) \rightarrow \pi^+\pi^- J/\psi$ decay distributions." Physical Review D 62 (2002): 032002.

[11] A. Rittenberg. Ph.D. thesis. University of California Radiation Laboratory, 1969.

[12] F. Butler *et al.*, (CLEO Collaboration). "Analysis of hadronic transitions in $\Upsilon(3S)$ decays." Physical Review D 49 (1994): 40-57.

[13] K. Hikasa *et al.*, (Particle Data Group). "Review of Particle Physics." Physical Review D 45 (1992): S1.

[14] T. Bowcock *et al.*, (CLEO Collaboration). "Study of $\pi^+\pi^-$ Transitions from the $\Upsilon(3S)$." Physical Review Letters 58 (1987): 307-10.

[15] E.A. Engelson, R.S. Galik, and D.L. Kreinick. "Analysis of Υ(3S)$\rightarrow$ Υ(1S) $\pi^0\pi^0$ and Υ(3S)$\rightarrow$ Υ(2S)$\pi^0\pi^0$." CBX in preparation. Presented at April 2003 APS meeting.

[16] L.S. Brown and R.N. Cahn. "Chiral Symmetry and $\psi' \rightarrow \psi\pi\pi$ Decay." Physical Review Letters 35 (1975): 1-4.

[17] M.B. Voloshin. "The Adler self-consistency condition in the decay $\psi(3700) \rightarrow \psi(3100)\pi\pi$." JETP Letters 21 (1975): 347-8.

[18] R.N. Cahn. "Angular distributions in the decay $\psi^- \rightarrow \psi\pi\pi$." Physical Review D 12 (1975): 3559-63.

[19] K. Gottfried. "Hadronic Trans. between Quark-Antiquark Bound States." Physical Review Letters 40 (1978): 598-601.

[20] H.Y. Zhou and Y.P. Kuang. "Coupled-channel effects in hadronic transitions in heavy-quarkonium systems." Physical Review D 44 (1991): 756-69.

[21] R.C. Giles and S.-H. Tye. "Application of the quark-confining string to the ψ spectroscopy." Physical Review D 16 (1977): 1079-95.

[22] M. Voloshin and V. Zakharov. "Measuring QCD Anomalies in Hadronic Transitions between Quarkonium States." Physical Review Letters 45 (1980): 688-91.

[23] V.A. Novikov and M.A. Shifman. Zeitschrift für Physik C Particles & Fields 8 (1981): 43.

[24] I.C. Brock *et al.*, (CLEO Collaboration). "Study of $\pi^+\pi^-$ transitions from the Υ(3S) and a search for the h_b." Physical Review D 43 (1991): 1448.

[25] T.K. Pedlar and S.P. Pappas. "Study of Dipion Transitions from Υ(3S) to Υ(1S) and Υ(2S) and Search for the h_b." CBX in preparation.

[26] D. Morgan and M.R. Pennington. "$\psi' \rightarrow \psi\pi\pi$ decay as a test of partial conservation of axial-vector current." Physical Review D 12 (1975): 1283-8.

[27] G. Bélanger, T. DeGrand, and P. Moxhay. "Spectra of the transitions $\Upsilon(nS) \rightarrow \Upsilon(mS)$ $\pi^+\pi^-$." Physical Review D 39 (1989): 257-65.

[28] P. Moxhay. "Coupled-channel effects in the decay Υ(3S)$\rightarrow$ Υ(1S)$\pi^+\pi^-$." Physical Review D 39 (1989): 3497-9.

[29] S.-K. Choi *et al.*, (Belle Collaboration). "Observation of a Narrow Charmoniumlike State in Exclusive $B^{\pm} \rightarrow K^{\pm}\pi^+\pi^- J/\psi$ Decays." Physical Review Letters 91 (2003): 262001.

[30] M. Artuso *et al.*, (CLEO Collaboration). "Photon Transitions in Υ(2S) and Υ(3S) Decays." Physical Review Letters 94 (2005): 032001.

[31] G. Bonvicini *el al.*, (CLEO Collaboration). "First observation of a $\Upsilon(1D)$ state." Physical Review D 70 (2004): 032001.

[32] S. Pappas (California Institute of Technology, Lauritsen Lab). Proceedings of the CLEO Collaboration summer PTA meetings. Cornell University, Ithaca, NY. 2003.

[33] H. Muramatsu and T. Skwarnicki, (CLEO Collaboration Internal Note). "Inclusive Photon Analysis in $b\bar{b}$ System." CBX 04-24 (2004): 1-38.

[34] T. Skwarnicki, (CLEO Collaboration Internal Note). "Study of Two-Photon Cascades in CLEO-III Υ(3S) Data." CBX 02-20 (2002): 11.

[35] H. Muramatsu and T. Skwarnicki, (CLEO Collaboration Internal Note). "Photon Transitions From $\psi(2S)$." CBX 03-32 (2003): 1-50.